Compendium

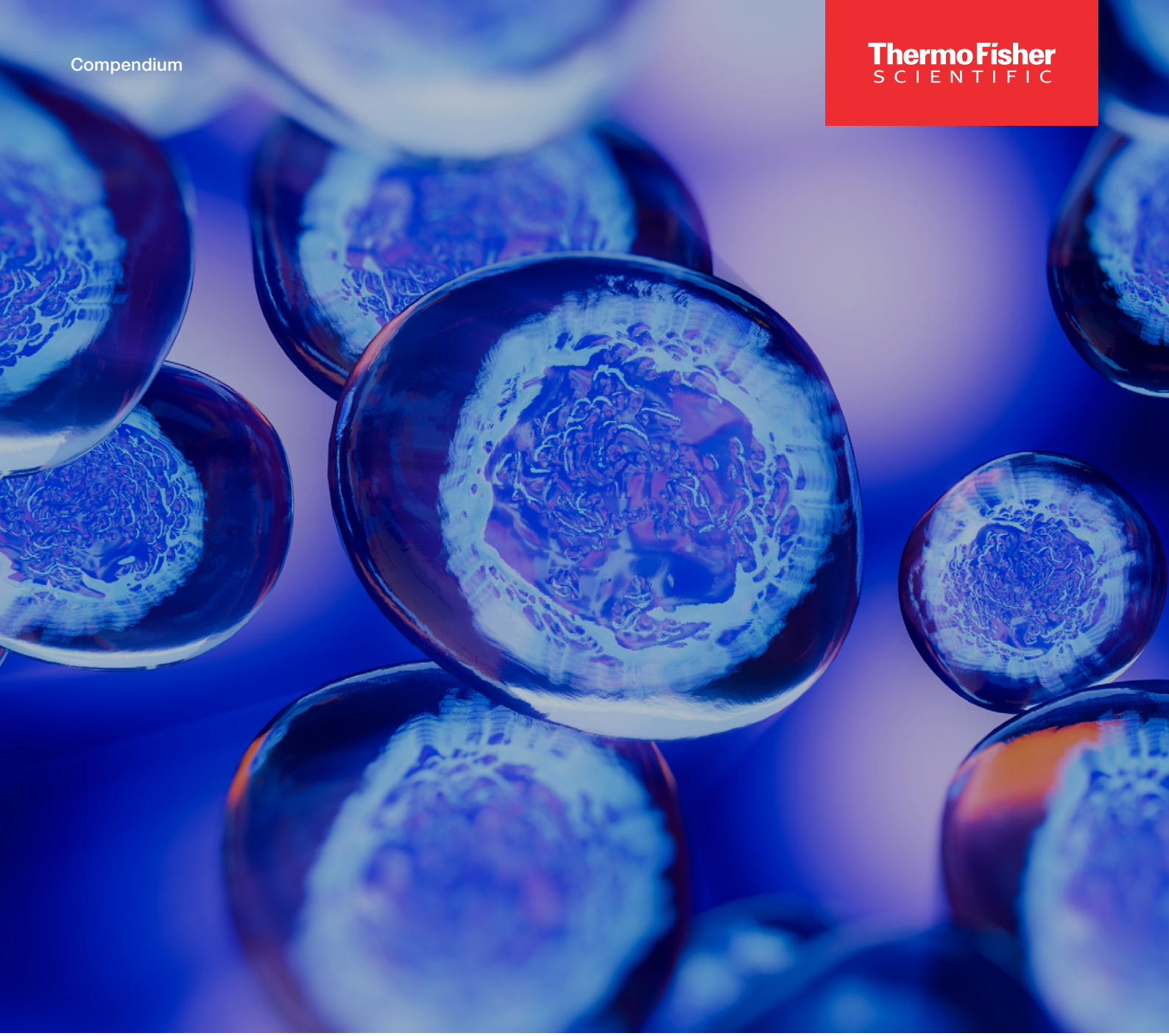

BioPharmaceutical approach with spectroscopy

thermo scientific

Summary

Heavily-regulated biopharmaceutical manufacturers are increasing their use of the molecular spectroscopy techniques mid-infrared (MIR), near infrared (NIR), and Raman UV-Vis spectroscopy because of these techniques' rapid, accurate analysis capabilities and their complementary nature. MIR spectroscopy is the analytical tool of choice for material verification in small molecule manufacturing due to its simplicity of implementation and its reliability and specificity. Recently, Raman spectroscopy has gained popularity in large molecule manufacturing, since it has increased sensitivity because of the resonance enhancement caused by the large size of molecules, as well as sensitivity to polymorphism. For certain applications like positive raw material verification of protein purification resins, the use of photoacoustic spectroscopy with Fourier-transform infrared (FTIR) offers unique selectivity and sensitivity. Vibrational spectroscopy plays a major role for analysis in upstream, downstream, and fill-finish processes. To support upstream processes, MIR, NIR, and Raman spectroscopy can be utilized for multi-attribute raw material testing. Further, in downstream processing, critical quality attributes (CQAs) like glycosylation, aggregation, and degradation can be determined at line or inline using Raman spectroscopy. Recently, NIR spectroscopy was demonstrated to have a wide variety of potential applications to improve speed and efficiency in different downstream unit operations, including capture chromatography, protein PEGylation reactions, and tangential flow ultrafiltration.

Real-time release testing (RTRT) in biopharmaceutical manufacturing has increasing importance. In this regard, macro-Raman measurements through primary packaging offer faster alternative tests for CQAs like pH, osmolality, and potency (strength), along with the positive identification of the drug product.

In addition, identification can be accomplished with macro- and micro-Raman spectroscopy in lyophilized biopharmaceutical analysis of cake morphology, siliconization, distribution of the drugs along with foreign particulate.

Currently, CQAs such as moisture and potency are commonly determined using destructive and time-intensive techniques like Karl Fischer titration. Since NIR spectroscopy is very sensitive to moisture, employing NIR for such analysis allows accurate and repeatable analysis of lyophilized cake through glass vials or containers in less than a minute.

Another technique, UV-Vis spectroscopy is used for quantitative analysis across the biopharmaceutical industry. Applications range from quantifying small volumes of genomic material to assessing protein aggregation in large volume samples. Accurate quantitation is a critical step within R&D and QA/QC.

Table of Contents

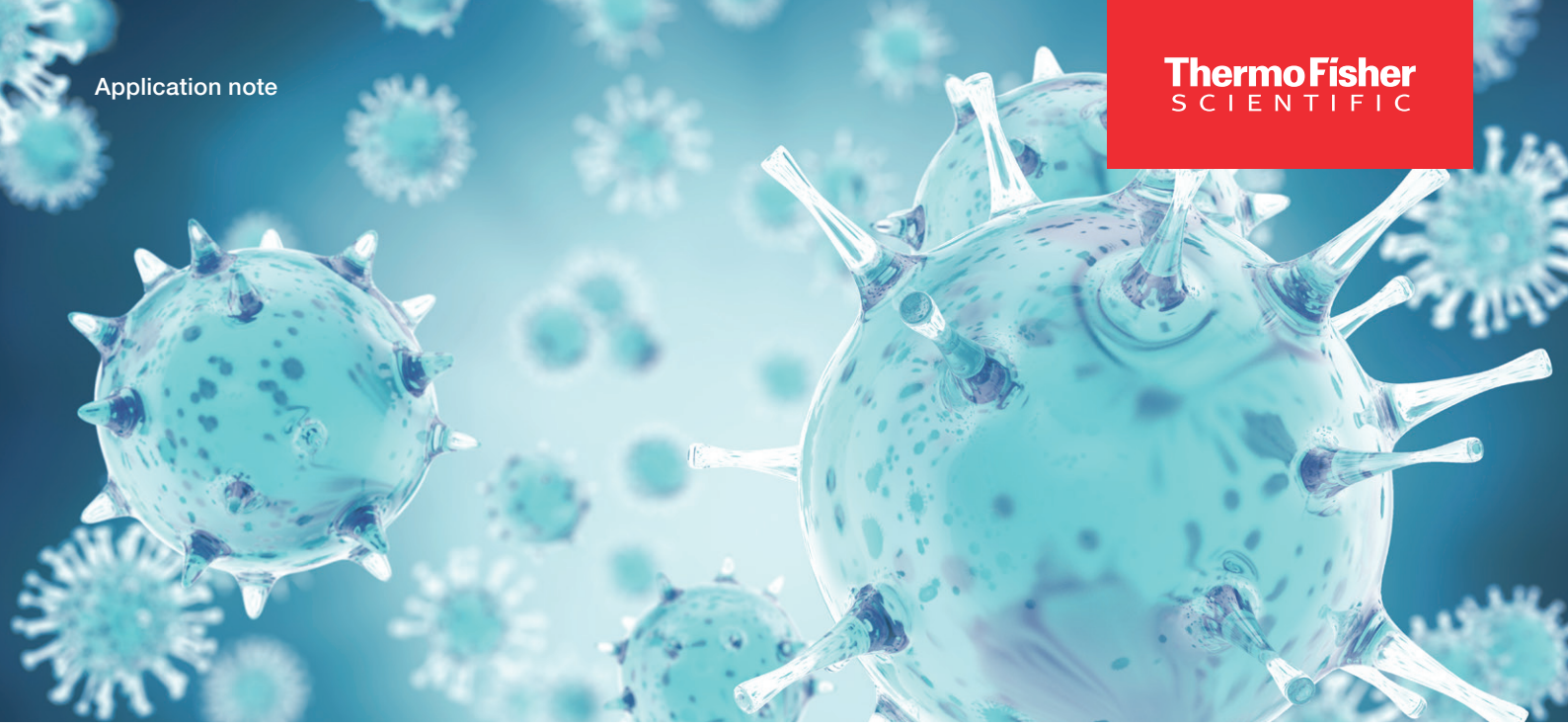

Application note

Protein secondary structure elucidation using FTIR spectroscopy

Author

Suja Sukumaran

Thermo Fisher Scientific, USA

Keywords

FTIR, ATR, protein structure elucidation, Biocell calcium fluoride cell, ConcentrateIR2 ATR, transmission

Abstract

Fourier-transform infrared (FTIR) spectroscopy is one of the most versatile analytical tools used across various disciplines. In this study, the Thermo Scientific™ Nicolet™ iS10 and Nicolet iS50 FTIR Spectrometers, equipped with attenuated total reflection (ATR) FTIR and transmission FTIR, were used for the determination of protein secondary structures. Structure calculations based on a protein database as well as spectral deconvolution are discussed. The analyses were quick and easy.

Introduction

Protein secondary structure describes the repetitive conformations of proteins and peptides. There are two major forms of secondary structure, the α-helix and β-sheet, so named for the patterns of hydrogen bonds between amine hydrogen and carbonyl oxygen atoms that create the peptide backbone of a protein.[1] Understanding protein secondary structure is important to gain insight into protein conformation and stability. For example, temperature dependent analysis of the secondary structure is critical in determining storage conditions for maintaining active therapeutic proteins.[2] Protein secondary structure is also crucial in understanding the structure–function relationship and enzyme kinetics of various proteins.[3]

FTIR has long been established as a powerful analytical technique to investigate protein secondary structure and local conformational changes.[1, 4] A typical protein infrared (IR) spectrum often contains nine amide bands, with vibrational contributions from both protein backbone and amino acid side chains. Among which, of particular pertinence to protein secondary structure are amide I and amide II bands. The absorptions associated with C=O stretching are denoted as amide I, whereas those associated with N–H bending are amide II. Since both C=O and N–H bonds are involved in the hydrogen bonding between different moieties of secondary structure, the positions of both amide I and amide II bands are sensitive to the secondary structure composition of a protein,[3, 4] although the amide II band is widely viewed as a less useful predictor for quantifying the secondary structure of proteins.

The shifts in the amide I band are often small compared to the intrinsic width of the band, resulting in one broad peak instead of a series of resolved peaks for each type of the secondary structure. Mathematical procedures such as Fourier self-deconvolution and second derivatives can be used to resolve the overlapping bands for the quantitative analysis of protein secondary structure.[3] Table 1 shows the secondary structure band assignments for proteins in water. Note that all assignments are depicted as a range, as the exact position of each peak varies from protein to protein due to the differences in hydrogen bonding interactions and the environment of the proteins.

Secondary structure	Band assignment in water
α-Helix	1,648–1,657 cm^{-1}
β-Sheet (high-frequency component)	1,623–1,641 cm^{-1} 1,674–1,695 cm^{-1}
Random	1,642–1,657 cm^{-1}
Coils	1,662–1,686 cm^{-1}

Table 1. Secondary structure band assignments for protein in water.[2]

With a range of sampling techniques, including transmission, ATR, and infrared reflection absorption spectroscopy (IRRAS), FTIR is particularly advantageous in terms of its versatility and general applicability compared to other analytical techniques for protein secondary structure analysis. Protein sample forms suitable for FTIR analysis include lyophilized powders, water solution, and colloids, to name a few. We report herein two examples of protein secondary structure determination using transmission FTIR and ATR, respectively. Both methods are fast, consume a minute amount of sample, and require minimal sample preparation.

Experiment

All proteins were procured from Sigma-Aldrich (MO, USA) and used as received. For the transmission studies, a BioCell™ Calcium Fluoride Cell (Biotools, Jupiter, FL) was used, and all measurements were carried out at ambient temperature. A 10 µL protein solution was placed at the center of the window, and the protein solution was sandwiched between the two CaF_2 windows, and placed in the holder. The concentration of protein tested was between 6 and 12 mg/mL. A 6 µm path length was created by sandwiching the two CaF_2 windows. CaF_2 windows are suited for water-based sample analysis. As water has a significant absorption peak at 1,645 cm^{-1} region, a small path length of 6 µm can effectively avoid saturated water peaks.

A purged Nicolet iS10 FTIR Spectrometer, equipped with a DTGS detector, was used for transmission analysis. The scan parameters used were 256 scans with a resolution of 4 cm^{-1}. The Thermo Scientific Smart OMNI-Transmission™ Accessory allows for a quick purge of the chamber, eliminating the need for water vapor subtraction in most analyses. Secondary structure analysis of the buffer-subtracted spectra was carried out using the built-in feature of the PROTA-3S™ FT-IR Protein Structure Analysis Software. Secondary structure calculation in PROTA-3S software is based on a database of 47 secondary structures (for more information visit www.btools.com).

For ATR analysis, a ConcentratIR2™ Multiple Reflection ATR Accessory (Harrick Scientific Products, Inc. Pleasantville, NY) with diamond crystal was used in a Nicolet iS50 FTIR spectrometer equipped with a mercuric cadmium telluride (MCT) detector. The diamond ATR has ten internal reflections with a nominal angle of incidence of 45 degrees. A 10 µL protein solution in phosphate buffer was dried on the surface of the ATR crystal under a stream of nitrogen. Scan parameters used were 256 scans and a resolution of 4 cm^{-1}. Secondary structure determination was carried out using the peak resolve feature of the OMNIC™ Software.

Results and discussion

Transmission-FTIR with Bio Cell

Figure 1 shows the overlay of three FTIR spectra: phosphate buffer, cytochrome C at 6 mg/mL and 12 mg/mL in phosphate buffer, respectively. At first glance, the spectra are predominantly water bands. The three spectra show little difference, even at a high protein concentration of 12 mg/mL.

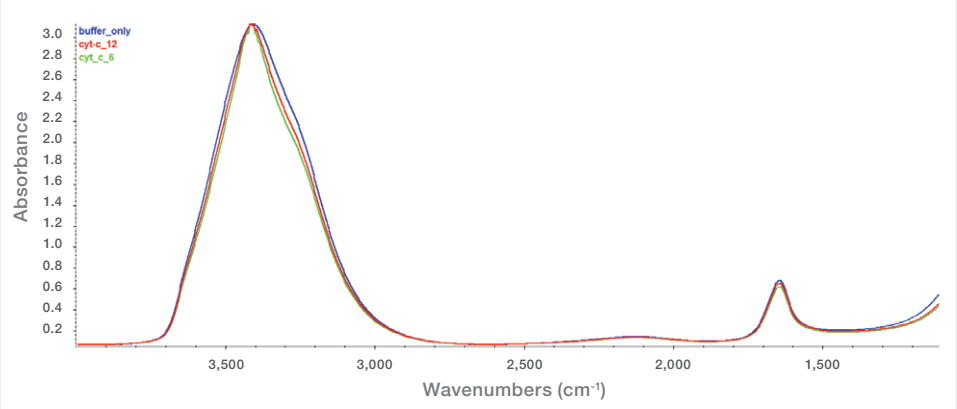

Figure 1. Transmission-FTIR spectra for cytochrome C in phosphate buffer (cytc_12) at 12 mg/mL and 6 mg/mL (cytc_6), and phosphate buffer blank.

Next, the buffer spectrum was subtracted from the raw protein spectra using the PROTA-3S software, and the results are shown in Figures 2A (cytochrome C) and 2B (concanavalin). The amide I and II peaks are clearly discernible in both spectra. The amide I peak position for cytochrome C spectra is 1,654 cm^{-1}, suggesting an α-helix dominant secondary structure. For concanavalin A, the amide I peak centers at 1,633 cm^{-1}, and there is also a noticeable shoulder peak at 1,690 cm^{-1} (red circle), indicative of the β-sheet component and its associated high-frequency component.[2]

Table 2 summarizes the secondary structure prediction using the PROTA-3S software. The cytochrome C has 45% α-helix and 5% β-sheet, whereas concanavalin A has 42% β-sheet and 4% α-helix. Differences in secondary structure composition between X-ray and FTIR data are likely due to the physicochemical state of the protein samples such as crystalline versus solution, temperature, pH, buffer conditions, etc. Furthermore, different prediction algorithms could have slightly varying outputs.[7] Notwithstanding the differences in analytical technique, sample state, and prediction algorithms, the secondary structure elucidation by FTIR using PROTA-3S software is largely in line with that from X-ray. Transmission-FTIR measurements combined with PROTA-3S software offer a facile and fast means to analyze the secondary structure of proteins in solution[2, 3] with minimal sample prep.

ATR-FTIR with ConcentratIR2 Accessory

When the quantity and concentration of protein are limited, FTIR measurements with the ConcentratIR2 Multiple Reflection ATR offer a better alternative than transmission-FTIR spectroscopy. The unique design of this ATR accessory allows for the direct measurement of protein powders, gels, solutions as well as proteins dried on the ATR surface. When concentrating proteins on the crystal surface, caution should be exercised in buffer selection since buffer will also concentrate on the surface of the crystal.

Only those buffers with minimum or no peaks in the amide I and II region should be selected. Figure 3 shows the ATR-FTIR spectra of BSA in phosphate buffer, dried on the crystal from a 1 mg/mL solution. In addition to the amide I and II bands, there are spectral features of the side chain, such as 1,515 cm^{-1} from tyrosine and 1,498 cm^{-1} from aspartic acid. Side chain peaks are critical for the elucidation of protonation and de-protonation states of various amino acids.[2]

	α-Helix (%)		β-Sheet (%)		Random (%)	
Protein	FTIR	X-ray	FTIR	X-ray	FTIR	X-ray
Cytochrome C	45	41	5	0	50	59
Concanavalin A	4	0	42	48	54	52

Table 2. Comparison of secondary structure calculation from FTIR (PROTA-3S) and X-ray data.

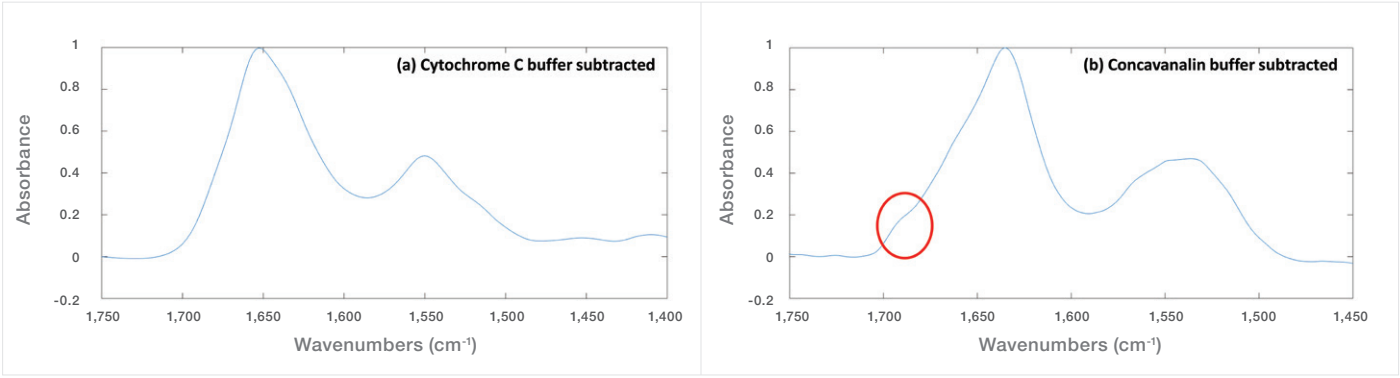

Figure 2. FTIR spectra of (a) cytochrome C and (b) concanavalin A after the buffer spectrum was subtracted using PROTA-3S software.

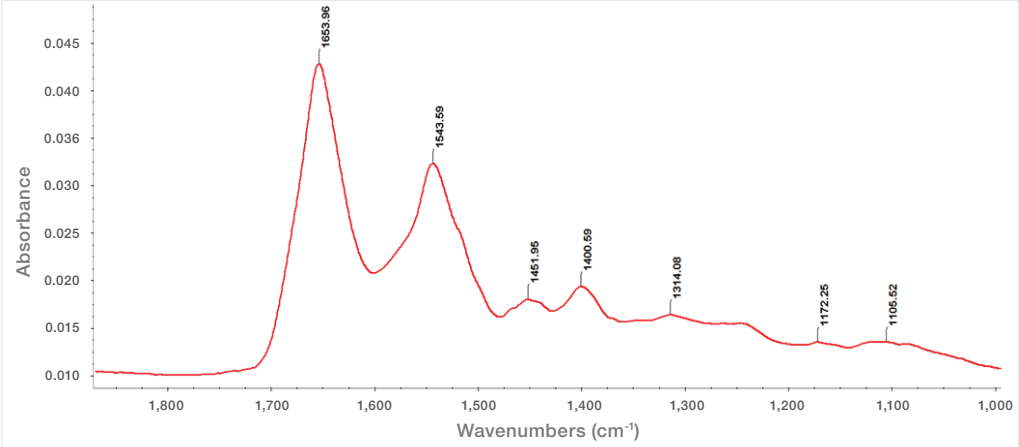

Figure 3. Amide I and II for 1 mg/mL BSA analyzed using ConcentratIR2 ATR on the Nicolet iS50 FTIR Spectrometer equipped with an MCT detector.

Peak deconvolution of the amide I peak (Figure 4) of BSA was carried out using the OMNIC software. It is important to note that second derivative analysis is often performed prior to deconvolution to clearly identify the peaks required for peak fitting.[2] In the current study, the second derivative peaks obtained (results not shown) are well correlated to the secondary structure peak assignments in Table 1. In order to obtain a good peak shape for peak fitting, a baseline correction on the amide I region was also performed. Baseline correction also effectively excluded the contributions from the amide II region. The deconvolution of amide I resulted in 5 peaks, and the area under each peak was then evaluated against the total area. Amide I peak deconvolution shows a secondary structure composition of 47% α-helix, 3% β-sheet, 24% coils, and 26% random, which is to published FTIR5 and X-ray data.

Conclusion

In this note, we have demonstrated two examples of protein secondary structure elucidation using FTIR spectroscopy. Transmission-FTIR measurements combined with PROTA-3S software provides a facile means to analyze secondary structure of proteins in solution with minimal sample preparation. When the quantity and concentration of protein are limited, ATR-FTIR offers a better alternative by drying the proteins in ATR crystals directly. The data were collected using an older model, the Nicolet iS10 Spectrometer. An improved model, the Nicolet iS20 Spectrometer, offers superior speed and performance over this predecessor model.

References

1. Elliott, A., Ambrose, E. J. **Structure of synthetic polypeptides**, Nature (1950) 165, 921-922.
2. Jackson, M., Mantsch, H.H. **The use and misuse of FTIR spectroscopy in the determination of protein structure**, Crit. Rev. Biochem. Mol. Biol. (1995) 30, 95-120.
3. Barth, A. **Infrared spectroscopy of proteins**, Biochim. Biophys. Acta (2007) 1767, 1073-1101.
4. Byler, D.M., Susi, H. **Examination of the secondary structure of proteins by deconvolved FTIR spectra**, Biopolymers (1986) 25, 469-487.
5. Surewicz, W.K., Mantsch, H.H. **New insight into protein secondary structure from resolution-enhanced infrared spectra**, Biochim. Biophys. Acta (1988) 952, 115-130.
6. Sukumaran, S., Hauser, K., Maier, E., Benz, R., Mantele, W. **Tracking the unfolding and refolding pathways of outer membrane protein porin from Paracoccus denitrificans**, Biochemistry (2006) 45, 3972–3980.
7. Klose, D., Janes R.W. 2Struc – **the protein secondary structure analysis server**, Biophysical Journal (2010) 98, 454-455.

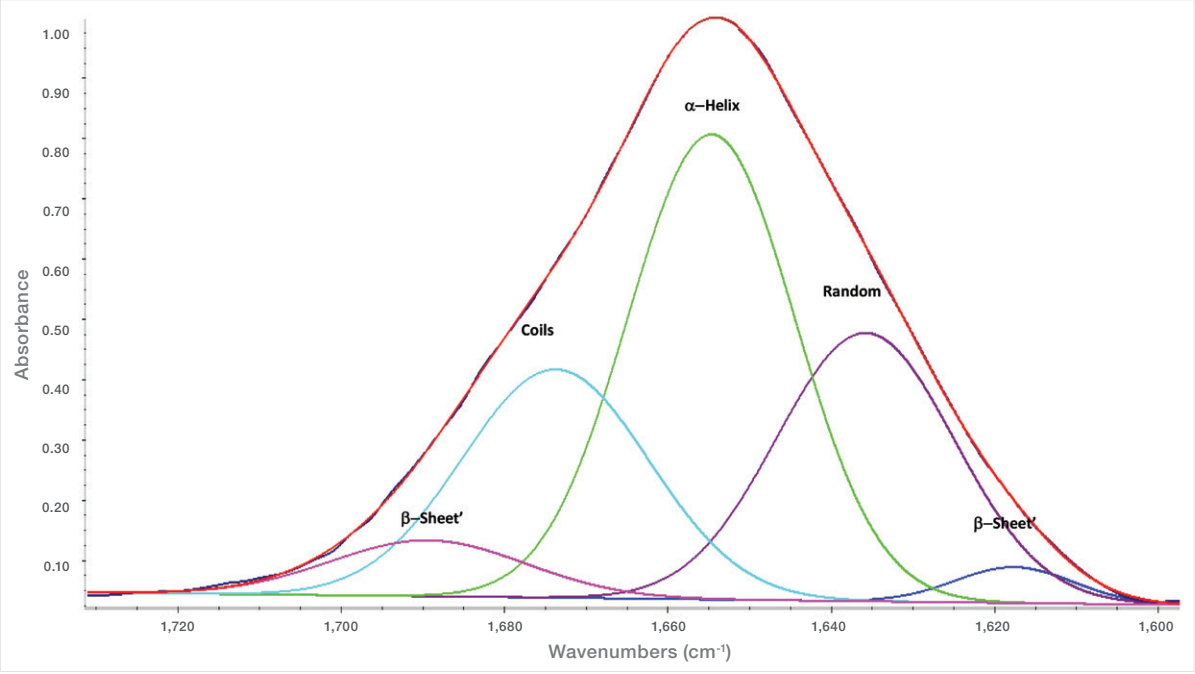

Figure 4: Peak deconvolution of amide I peak of BSA using Peak Resolve function of OMNIC software.

Learn more at **thermofisher.com/brighteroutcomes**

thermo scientific

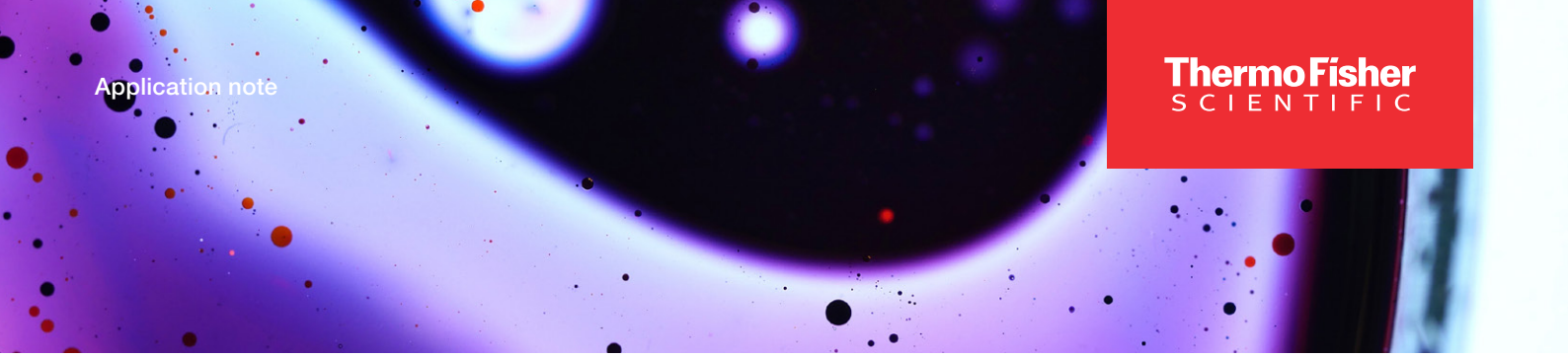

Protein concentration prediction in cell cultures

The next stage in NIR bioprocess analysis

Author

Todd Strother, PhD, Thermo Fisher Scientific, Madison, WI, USA

Figure 1. Antaris MX FT-NIR Process Analyzer used for collecting thespectroscopic information from the cell cultures.

Introduction

Biologically produced materials are an increasingly important aspect in many industrial processes including those related to pharmaceuticals, food, diagnostics, and fuels. Most of these biologicals are produced in fermentors and bioreactors in which specialized cell cultures grow and manufacture the molecule of interest. Many different types of cells are used in culturing and producing biopharmaceutical products including genetically engineered bacterial and yeast cells. However a majority of the products are proteins cultured from mammalian systems such as Chinese hamster ovary (CHO), green monkey (VERO), or human embryonic kidney (HEK) cell lines. Many of these products are large complex proteins, hormones or polysaccharides that are impossible or difficult to manufacture in large quantities any other way. A recent survey of the US Food and Drug Administration noted that there are over 350 biologicals approved for various uses, including vaccines and diagnostic and therapeutically important antibodies.

Bioprocesses that produce the desired materials by nature rely on complex biological systems to synthesize their useful products. While typical chemical manufacturing processes have relatively little variability, the inherent complexity of biological systems makes a great deal of variability from batch to batch inevitable. As a consequence of the complexity and variability of the processes, it has been estimated that 30% of the production batches need to be reprocessed for quality reasons, which results in a tenfold loss in profit. Industries that rely on these complex biological systems benefit greatly from closely monitoring the growth of their cell cultures and production of the target molecule. Process analytical technology (PAT) initiatives in bioprocesses improve the overall product quality, reducing waste by accounting for this inherent variability.

Monitoring and controlling cell culture conditions greatly reduces this variability and results in improved target protein production. Fourier transform near-infrared (FT-NIR) spectroscopy has proven to be a useful technology for monitoring and controlling manufacturing processes including more specific bioprocess applications. It is also part of PAT initiatives across many industries including bioprocessing. Previous work performed on cell cultures using NIR spectroscopy has usually focused on monitoring and controlling nutrients, waste products, cell densities and other parameters related to the health of the cell culture. While these parameters are useful for determining the relative health of the cell culture, the more important parameter of interest is the actual production and concentration of the target molecule. Very few NIR studies have determined and measured protein concentrations in actual cell culture conditions. This application note demonstrates the feasibility of using the Thermo Scientific™ Antaris™ MX FT-NIR Process Analyzer (Figure 1) to predict protein concentrations at biologically relevant concentrations in dynamic cell cultures.

NIR spectroscopy uses light between 10,000 and 4,000 cm^{-1} to determine the identity and quantity of a variety of materials. Most molecules of interest absorb light in this region through combination or overtone vibrations. The advantage of performing spectral analysis on these absorption bands is that the light is able to penetrate more deeply into the material under analysis and does not require dilution or manipulation of the sample. Therefore NIR analyzers can be coupled directly into a process stream or tank where spectral analysis can be performed without human intervention. FT-NIR has been implemented in many different industrial, pharmaceutical and other process settings for many years and has proven to be extremely valuable in collecting real-time analytical data automatically. When used in process environments, the Antaris MX FT-NIR Process Analyzer is easily coupled to process control computers where it is an integral part of maintaining optimal manufacturing conditions. Because of these advantages and the need to control the inherently variable biological systems found in cell culture technologies, NIR is an excellent choice for analyzing different components in bioreactors including proteins.

Methods

Chinese hamster ovary (CHO) cell cultures were grown at optimal conditions until the cell concentrations reached approximately one million per millemeter, representing a typical cell density for a young and growing culture. Samples of the cell culture were tested on a Nova BioProfile® analyzer to determine concentrations of glucose, glutamine, lactate, and ammonia. The concentrations of these materials changed throughout the experiment and accounted for some variability that might be encountered across multiple cultures. The concentrations were variously and singularly altered by spiking the samples with nutrients or waste products or diluting the samples with unaltered cell culture. Each of those four components was altered so that two or three different concentrations were represented for each. Table 1 lists the concentration ranges for the various nutrient, waste, and protein components of the tested samples. This methodology also has the effect of removing covariance between the different components and protein present.

Component	Range (g/L)
Protein	0.16–5.00
Glucose	7.98–8.12
Glutamine	0.28–0.58
Lactate	0.45–0.90
Ammonia	0.05–2.39

Table 1. Concentration ranges of various components. The solutions represent over 35 different protein concentrations that also vary in concentrations of nutrient and waste components.

Ultrapure bovine albumin protein was added to the solutions to represent target protein synthesized by the cells. Genetically modified cell cultures are designed to produce the target protein in large quantities almost exclusively to all other cellular proteins. As a result, the protein concentrations in the cell culture media will often approach and exceed 5.0 g/L and consist almost entirely of the target molecule. Albumin protein is an excellent mimic for recombinant proteins because it is available in extremely pure form and contains NIR active groups essentially identical to a typical target protein from a cell culture. In this case, purity is extremely important because any extraneous material present will also have a NIR signal and would lead to confounding results. The albumin protein material was carefully weighed and added to the cell cultures in concentrations ranging from 0.16 to 5.0 g/L. Over 35 different solutions were produced that had a range of nutrient and waste as well as protein concentrations. These varied solutions resulted in 54 spectra that were used to build the chemometric method and 20 spectra that were used to validate that method.

The cell culture samples were scanned with an Antaris MX FT-NIR Process Analyzer in the range between 10,000 and 4,000 cm^{-1}. The analyzer was coupled to a transflectance probe with an adjustable path length. The gap distance was set to 1.25 mm for a total path length of 2.5 mm. Sixteen scans were averaged per spectrum and were collected using eight wavenumber resolution with a gain of 0.1. Sample time took approximately 15 seconds. Two spectra were collected per sample. Figure 2 shows images of the probe before insertion into a cell culture sample and during spectral collection.

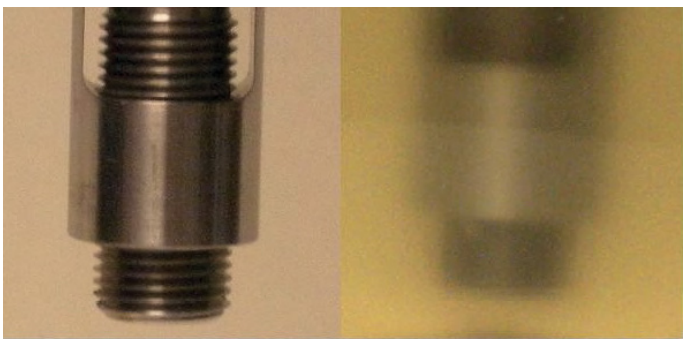

Figure 2. Transflectance probe used for data collection. Left panel shows the design of the probe with the adjustable pathlength. Right panel shows probe inserted into cell culture during data collection.

The sample spectra were loaded into the Thermo Scientific TQ Analyst™ Pro Edition Software for chemometric analysis using a partial least squares (PLS) method with a constant pathlength. The spectra were analyzed in the first derivative using a Norris smoothing filter. Two regions were used for the analysis: 8,910 to 5,340 cm^{-1} and 4,830 to 4,340 cm^{-1} These two regions collected information across a wide range of data points while avoiding the totally attenuating water peak centered around 5,100 cm^{-1}. Figure 3 shows representative raw spectra and the first derivative spectra of the samples.

Results

PLS analysis of the protein concentrations in the various cell culture samples revealed excellent predictive capabilities within the range of materials tested. The 54 spectra used to develop the PLS method are shown on a calibration plot (Figure 4) that compares the calculated protein concentrations versus the actual concentrations.

The calibration plot can be used to determine how well the method predicts the actual protein concentrations in the samples. The plot developed by the chemometric method resulted in a correlation coefficient of 0.977. Root mean square error of calibration (RMSEC) was 0.33 g/L and the Root mean square error of prediction (RMSEP) calculated from the 20 validation samples was 0.31 g/L. Additionally, the Root mean square error of cross validation (RMSECV) was 0.51 g/L. These errors indicate that the protein concentration in the cell culture samples can be predicted to 0.5 g/L or less. Approximately 1/3 of this error was attributed to the balance used to weigh the protein material.

Conclusions

Measuring protein concentrations in living dynamic cell cultures was successfully performed with the Antaris MX FT-NIR Process Analyzer. Protein concentration is a critical parameter in determining the success and quality of a cell culture in manufacturing a viable end product. This NIR technique successfully demonstrates the ability to measure and monitor protein concentrations in real time at relevant concentrations. The developed method shows excellent correlation with actual protein concentrations between 0.16 and 5.0 g/L and with errors of less than 0.5 g/L.

This application demonstrates the continued capability of the Antaris MX FT-NIR Process Analyzer to be successfully used in bioprocess environments where it can safely, accurately and automatically monitor and control cell cultures. While previous NIR studies have monitored cell culture conditions to promote optimal protein production, few have actually monitored and predicted protein concentrations. This feasibility study shows the power of the Antaris MX FT-NIR Process Analyzer to correctly predict target protein concentrations in a live and dynamic cell culture.

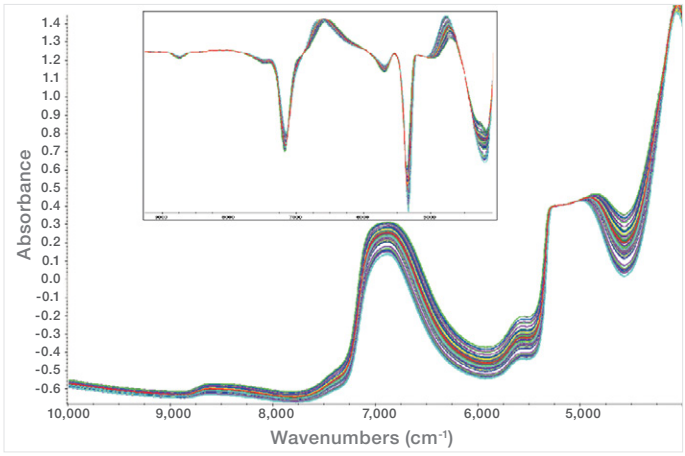

Figure 3. Representative raw spectra showing the variability present in the cell culture samples. Regions of analysis avoided the attenuated water peak at 5,100 cm^{-1}. Inset shows the first derivative spectra used for the PLS chemometric method.

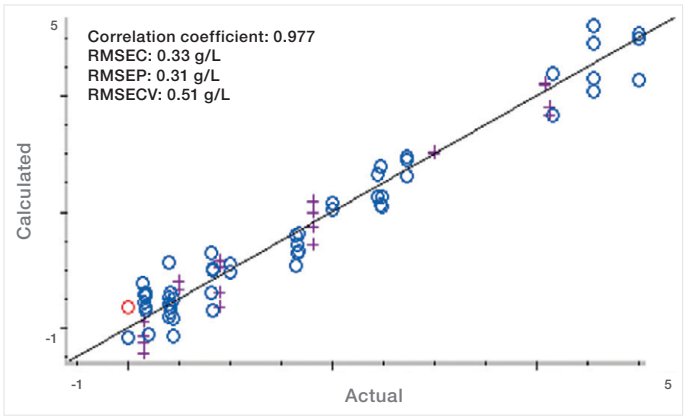

Figure 4. Calibration plot comparing the calculated protein concentrations to the actual concentrations from the PLS method. Root mean square errors are approximately 0.5 g/L or less. Blue circles (o) represent spectra used to create the method, purple crosses (+) are spectra used to validate the method.

Learn more at **thermofisher.com/brighteroutcomes**

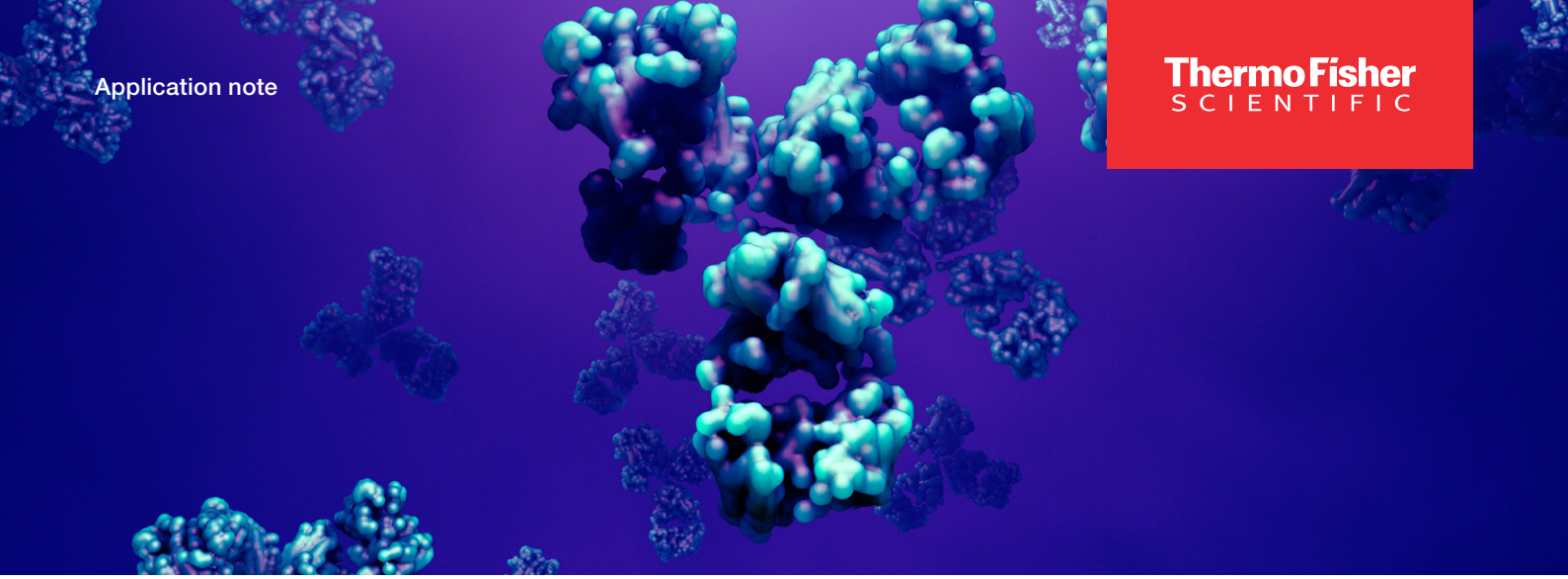

Application note

Protein aggregation identified through UV-Visible absorption spectroscopy

Introduction

Misfolded or denatured proteins can associate in solution,[1] forming insoluble aggregates (Figure 1). This process is often irreversible, effectively removing useful proteins from solution and making the detection of aggregates critical for further downstream use of protein solutions. This is particularly important when studying unstable or abnormal proteins, which are more likely to form aggregates.[2,3]

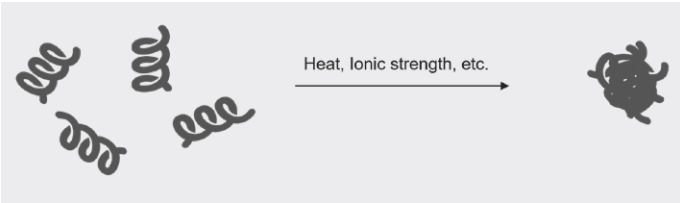

Figure 1. Visualization of protein aggregation induced by heat or changes in ionic strength.

The formation of protein aggregates in the body has also been linked to several diseases, including Alzheimer's and Parkinson's disease.[1,4,5] In the pharmaceutical industry, protein therapeutics, such as insulin,[6] have been developed to effectively treat a variety of diseases but have been difficult to synthesize.[7] The presence of aggregates in these products can lead to lower product yields and can reduce the efficacy of the final therapeutic.[5, 8] For example, protein therapeutics that undergo aggregation have been linked to lowered immune responses and, in some cases, can even induce allergic reactions.[8]

In the food industry, protein composition can have a large impact on the palatability of the final product. Protein aggregates can significantly change a food's organoleptic properties (e.g., taste, smell, etc.), as well as the digestibility of the material.[5]

Size-exclusion chromatography has previously been used to identify the presence of aggregates in a sample.[9] This characterization method is time-consuming, however, and sample retrieval can be difficult. An alternative method for the detection of protein aggregates uses UV-visible (UV-Vis) absorption spectroscopy, a technique that measures a sample's light absorption. Aggregates in solution are known to scatter incoming light, resulting in an apparent absorption artifact across the entire spectrum.[5, 10] This scattering artifact does not represent the true absorption of the sample and instead indicates that the solution contains aggregates large enough to scatter the incoming light.

In this application note, UV-Vis absorption spectroscopy was used to identify the presence of protein aggregates in aqueous bovine gamma globulin (BGG) samples. Aggregation was induced in these samples using heat or the addition of NaCl. An integrating sphere was further used to measure the scatter-free spectra of the samples. Scatter-correction methods were used to determine the concentration of free, non-aggregated BGG in solution.

Experimental

Absorption spectra were collected using a Thermo Scientific™ Evolution™ One Plus UV-Vis Spectrophotometer. Samples were held in a 10 mm quartz cuvette, and measurements were collected between 220 and 400 nm. A stock 1.1 mg/mL BGG solution was made by diluting standard Thermo Scientific Pierce™ BGG Standard (2.0 mg/mL, Lot Number MH162604) with phosphate buffer (PBS, 1×) to achieve the appropriate concentration. A 5.3 M NaCl solution in phosphate buffer was made by dissolving 1.5 g NaCl (Fisher Scientific) in 6.0 mL of phosphate buffer. BGG samples were prepared as described in Table 1.

	BGG sample		Volume of 1.1 mg/mL BGG (mL)	Volume of PBS (mL)	Volume of 5.3 M NaCl (mL)
	Temperature (°C)	NaCl concentration (M)			
1	25.0	0.00	1.0	1.0	0.0
2	25.0	2.65	1.0	0.0	1.0
3	75.0 (60 min incubation)	0.00	1.0	1.0	0.0
4	75.0 (30 min incubation)	0.00	1.0	1.0	0.0

Table 1. BGG solution preparation.

BGG samples were heated using a single-cell Peltier accessory at 75°C for 30 or 60 minutes. Sample measurements were collected using a Thermo Scientific™ Evolution™ ISA-220 Integrating Sphere Accessory in transmission geometry. The collected data was reported using the Kubelka-Munk transformation. An 8° wedge was used for optimized light collection. After integrating sphere measurements were completed, Sample 4 (Table 1) was filtered using a syringe filter. The absorption spectrum of the filtrate was then measured using the Evolution One Plus Spectrophotometer, without the Evolution ISA-220 Accessory.

Results

The absorption spectrum of BGG (not aggregated), depicted in Figure 2a (blue curve), is in agreement with literature values.[11] Upon addition of NaCl, the entire spectrum appears to have a higher absorbance, an artifact resulting from the presence of larger particulates. Increased ionic strength of a protein solution (due to high salt concentration) has been shown to induce protein aggregation;[4] this scattering signal can therefore be attributed to the presence of small BGG aggregates. Scattering is observed regardless of the visual (clear, non-turbid) appearance of the solution (Figure 2c). This indicates that, while it is difficult to confirm through visual observation alone, aggregate scattering can be measured using UV-Vis absorption, and the technique can be used as a test for protein aggregation.

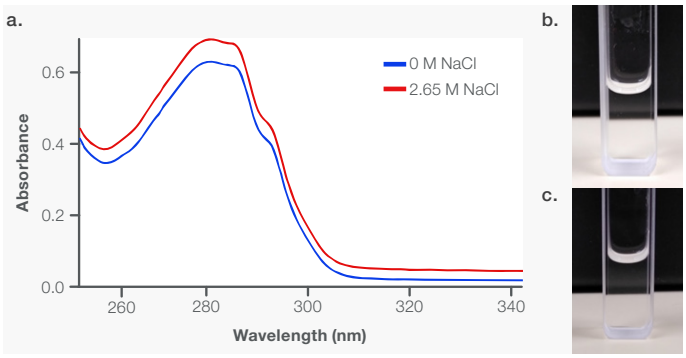

Figure 2. Absorption spectra of 0.55 mg/mL BGG in PBS with (red) and without (blue) 2.65 M NaCL. Images of a solution of BGG with (b) and without (c) 2.65 M NaCl.

Scattering appears as a raised baseline at longer wavelengths but also influences the apparent absorption across the entire spectrum and is highly dependent on the wavelength of the incident light. This influence can be estimated using the following equation:

$$A_{scatter} = \log (I_0/I_{no\ scatter}) + A_{offset} = \log (I_0/I_0\text{-}(f/\lambda^4))) + A_{offset} \quad (1)$$

In the equation above, $A_{scatter}$ is the scattering artifact/apparent absorption due to scattering, I_0 is the intensity of the light before it interacts with the sample, $I_{no\ scatter}$ is the intensity of the light that reaches the detector (not scattered by the solution), f is an arbitrary scaling factor, λ is wavelength in nanometers, and A_{offset} is an offset. This equation uses Beer's law,

$$A = \log (I_0/I) \quad (2)$$

and the relationship between the wavelength of light and the intensity of the scattered light, which is defined by the Rayleigh equation,[12]

$$I_{scatter} \propto (1/\lambda^4) \quad (3)$$

to determine an estimated intensity of the scattered light ($I_{scatter}$). Assuming I_0 is 1 and the intensity of the scattered light is less than 1, Equation 2 includes only two parameters that must be fit to determine the scattering contribution. The relationship between scattering intensity and wavelength indicates that there is a larger effect in the UV region (Figure 3a), where there are prominent absorption features for proteins. This effect must therefore be carefully corrected.

Figure 3b shows the data corrected using two different methods. The first, referred to as "baseline correction," involves taking the average of the absorption reported in the spectral region in which the sample should not absorb. The calculated average is then subtracted from each point in the spectrum, as described by:

$$A_{corrected,\lambda} = A_{measured,\lambda} - A_{average,(330\text{-}350\ nm))} \quad (4)$$

In this equation, $A_{measured\lambda}$ is the absorption spectrum collected, $A_{average,\ (330–350\ nm)}$ is the average of the absorption measured between 330 and 350 nm, and $A_{corrected\lambda}$ is the corrected absorption spectrum. The resulting spectrum is shown in Figure 3b (green curve); the maximum absorption from the band is still higher than that of the untreated BGG sample. This does not match the expected result, as formation of aggregates should remove free BGG from solution, leading to a lower concentration and lower absorbance in the region of interest. Consequently, the "baseline correction" does not properly account for the scattering artifact present in the collected spectrum.

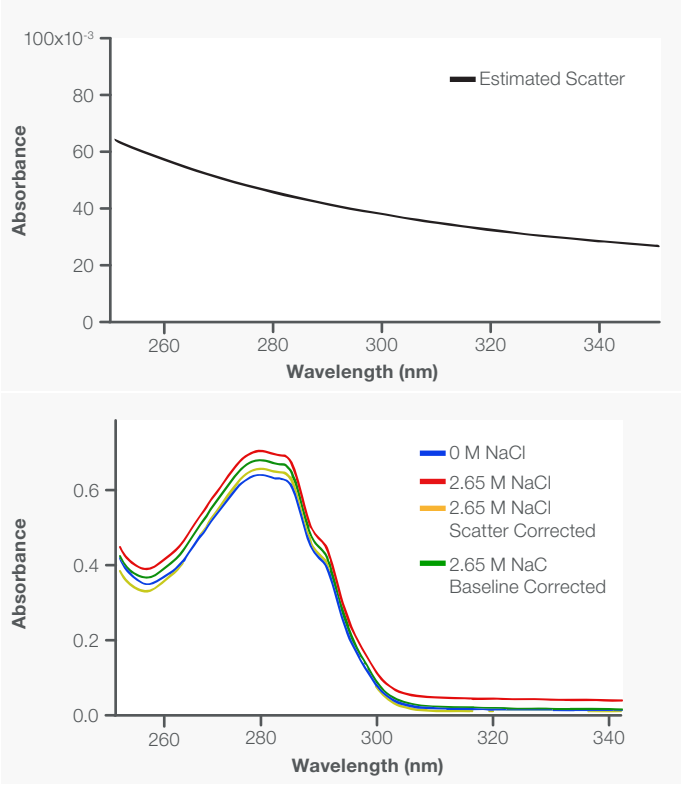

Figure 3. a) Estimated scattering calculated using Equation 1. b) Absorption spectra of BGG with and without NaCL. Baseline-corrected data is shown in green, calculated using Equation 4. Scatter-corrected data is shown in yellow, calculated using Equation 5.

The second method, called "scatter corrected", fits the long wavelength baseline to Equation 1, where f and A_0 are fit such that the resulting function matches the long wavelength signal well. The scattering function described in Figure 3a was fit using f = 6.1 x 10^8 and A_0 = 0.006. The resulting scatter function was then subtracted from the absorption spectrum, as shown in the following equation,

$$A_{(corrected,\lambda)} = A_{measured,\lambda} - A_{scatter,\lambda} \quad (5)$$

where $A_{scatter\lambda}$ is the calculated scatter estimate. This correction results in the yellow spectrum in Figure 3b. Unlike the baseline corrected spectrum (green curve, Figure 3b), the maximum absorption of the scatter-corrected spectrum is below the absorption maximum of the spectrum for untreated BGG, as expected.

The concentration of free, non-aggregated BGG in the sample was found to be 0.54 mg/mL using Beer's law:

$$A = c l \varepsilon \quad (6)$$

In the equation above, A is the measured absorbance, c is the concentration, l is the path length (1 cm), and ε is the extinction coefficient of the protein. Therefore, the concentration of proteins that contribute to aggregation in this sample is 0.01 mg/mL.

For samples with a relatively low scatter contribution, the mathematical scatter-correction method works well. However, for samples that are visibly cloudy/turbid, this correction is not ideal, as only a small portion of the light is allowed to interact with the detector. To study a sample that is turbid, a 0.55 mg/mL BGG sample was held at 75˚C for 60 minutes using a single-cell Peltier accessory for the Evolution One Plus Spectrophotometer, producing a cloudy solution (Figure 4b). The resulting absorption spectrum is depicted in Figure 4a. The scattering artifact present indicates that ~30% of the light is transmitted through the sample at 310 nm, where BGG begins to absorb, and even less is transmitted at shorter wavelengths. This suggests there is a high concentration of aggregates present in this heated sample.

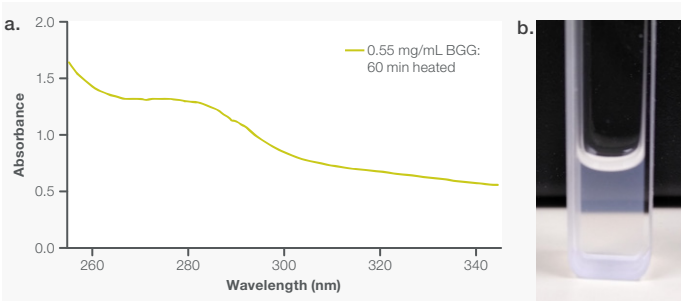

Figure 4. Absorption spectrum of 0.55 mg/mL BGG following a 60-minute incubation at 75˚C.

As mentioned previously, the small amount of light reaching the detector makes it difficult to mathematically correct for scattering. Instead, an integrating sphere can be used—this accessory allows for the collection of scattered light diffusely reflected off the inner walls of the sphere. As the diffuse light reflects many times, it can be uniformly collected, removing the scattering artifact. To correct for the scatter shown in Figure 4a, a spectrum for the aggregated BGG sample (Table 1, Sample 3) was collected using an Evolution ISA-220 Accessory. Through the instrument software, the signal was reported using Kubelka-Munk units, F(R), which is proportional to both the absorption coefficient, k, and scattering coefficient, s, of the material:

$$F(R)=k/s \quad (7)$$

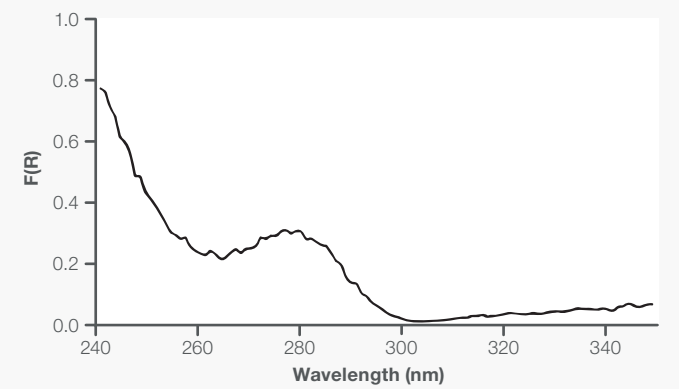

Figure 5. Kubelka-Munk spectrum of 0.55 mg/mL BGG after a 60-minute incubation at 75˚C.

Figure 5 demonstrates the Kubelka-Munk spectrum of the BGG solution shown in Figure 4; the scattering signal is largely removed from the spectrum.

F(R) is not equivalent to absorbance, indicating Beer's law cannot be used to determine concentration from the collected results. However, as F(R) is proportional to the absorption coefficient, it is also proportional to the absorbance, A, and the concentration, c, of the free proteins in solution:

$$F(R) \propto A \propto c. \quad (8)$$

To determine the concentration of aggregated and non-aggregated proteins in solution using the Kubelka-Munk formula, the fully non-aggregated sample (control) was measured using the integrating sphere. The resulting Kubelka-Munk spectrum collected is shown in Figure 6a (gray curve). A second BGG sample heated to 75˚C for 30 minutes (Table 1, Sample 4), which also resulted in a large scattering artifact, was analyzed using the Evolution ISA-220 Accessory as well.

If the collected F(R) of the sample at a given wavelength is assumed to be equivalent to the concentration of the proteins in solution multiplied by some constant, b, that is shared between all BGG samples, then we can construct a series of equations:

$$F_{control}(R) = c_{control} b \quad (9)$$

$$F_{sample}(R) = c_{sample} b \quad (10)$$

$$c_{sample} = c_{control} * F_{sample}(R)/F_{control}(R) \quad (11)$$

The equations above can be used to relate the concentration of non-aggregated BGG in the sample that was incubated at 75˚C (c_{sample}) to the concentration of the non-aggregated BGG control ($c_{control}$), the Kubelka-Munk signal of the sample ($F_{sample}(R)$), and the control ($F_{control}(R)$). For more complex samples, constructing a standard curve with multiple control samples of differing concentration would be a more effective analysis tool.

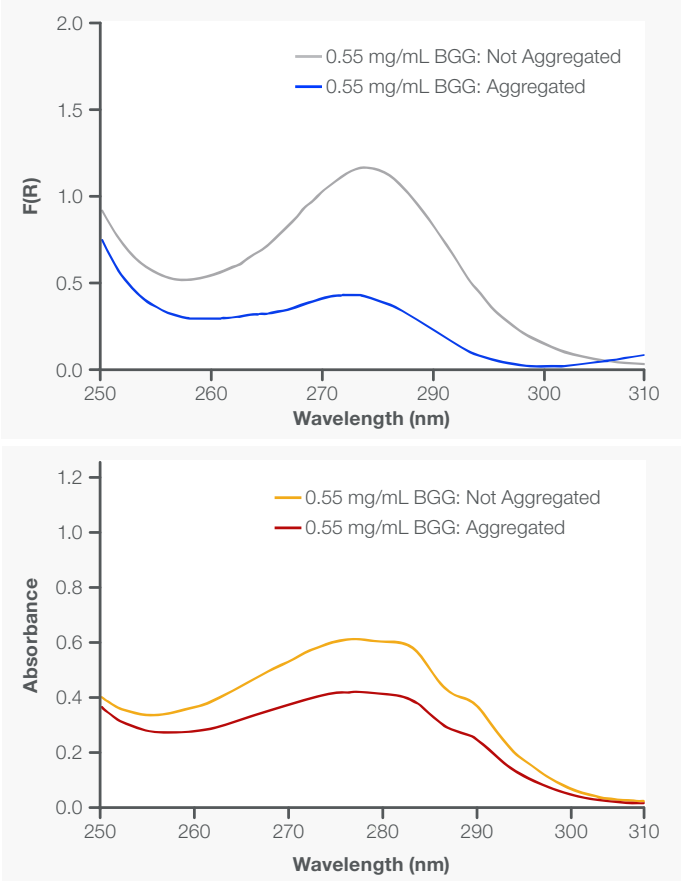

Figure 6. a) Kubelka-Munk spectra of 0.55 mg/mL BGG after a 30-minute incubation at 75˚C (blue) and 0.55 mg/mL non-aggregated BGG (gray). b) Absorption spectra of filtered 0.55 mg/mL BGG after a 30-minute incubation at 75˚C (brown) and 0.55 mg/mL non-aggregated BGG (orange). The incubated BGG sample was filtered using a Millipore Millex-GV PVDFA filter.

Using Equation 11, the concentration of non-aggregated materials in the BGG sample was found to be 0.20 mg/mL, implying 0.35 mg/mL of BGG contributed to the formation of aggregates in this sample. To verify this equation, the BGG sample containing aggregates was filtered using a syringe filter and the absorption spectrum of the filtrate was collected using a traditional cell holder. Using Beer's law, the concentration of the BGG filtrate was found to be 0.20 mg/mL, matching the calculated concentration determined using the integrating sphere. This further implies that BGG aggregates in solution do not absorb an appreciable amount of light in the spectral region of interest for this sample.

Conclusion

Protein aggregates in solution can quickly be detected using the Evolution One Plus UV-Visible Spectrophotometer. For samples with a low concentration of aggregate present, the resulting scattering artifact can be corrected by estimating the scattering contribution and subtracting that estimate from the measured spectrum. For highly scattering solutions, the Evolution ISA-220 Integrating Sphere Accessory works well in removing the scattering artifact from the spectrum. The concentration of free proteins in solution can then be solved for the corresponding spectrum of a known standard or a series of known standards.

References

1. Weids, A.J., Ibstedt, S., Tamás, M.J.; Grant, C.M., Sci. Rep. 2016, 6, 24554.
2. Chen, Z.; Huang, C.; Chennamsetty, N; Xu, X.; Li, Z.J., J. Chromatogr. A, 2016, 1460, 110 – 122.
3. Jubete, Y.; Maurizi, M.R., Gottesman, S., J. Biol. Chem., 1996, 271, 48, 30798-30803.
4. Da Vela, S.; Roosen-Runge, F.; Skoda, M.W.A.; Jacobs, R.M.J.; Seydel, T.; Frielinghaus, H.; Sztucki, M.; Schweins, R.; Zhang, F.; Schreiber, F., J. Phys. Chem. B 2017, 121, 23, 5759 – 5769.
5. Pignataro, M.F.; Herrera, M.G.; Dodero, V.I.; Molecules 2020, 25, 20, 4854.
6. Johnson, I.S., Science, 1983, 219, 4585, 632 – 637.
7. Mitragotri, S.; Burke, P.A.; Langer, R., Nat. Rev. Drug Discov., 2014, 13, 9, 655 – 672.
8. Lundahl, M.L.E.; Fogli, S.; Colavita, P.E.; Scanlan, E.M., RSC Chem. Biol., 2021, 2, 1004-1020.
9. Hawe, A.; Friess, W.; Sutter, M.; Jiskoot, W., Anal. Biochem. 2008, 38, 115 – 122.
10. Hall, D.; Zhao, R.; Dehlsen, I.; Bloomfield, N.; Williams, S.R.; Arisaka, F.; Goto, Y.; Carver, J.A., Anal. Biochem., 2016, 489, 78 – 94.
11. Smith, E.L.; Coy, N., J. Biol. Chem., 1946, 164, 1, 367 – 370.
12. Yao, G.; Li, K.A.; Tong, S.Y., Anal. Chim. Acta, 1999, 398, 319 – 327.

Learn more at **thermofisher.com/evolution**

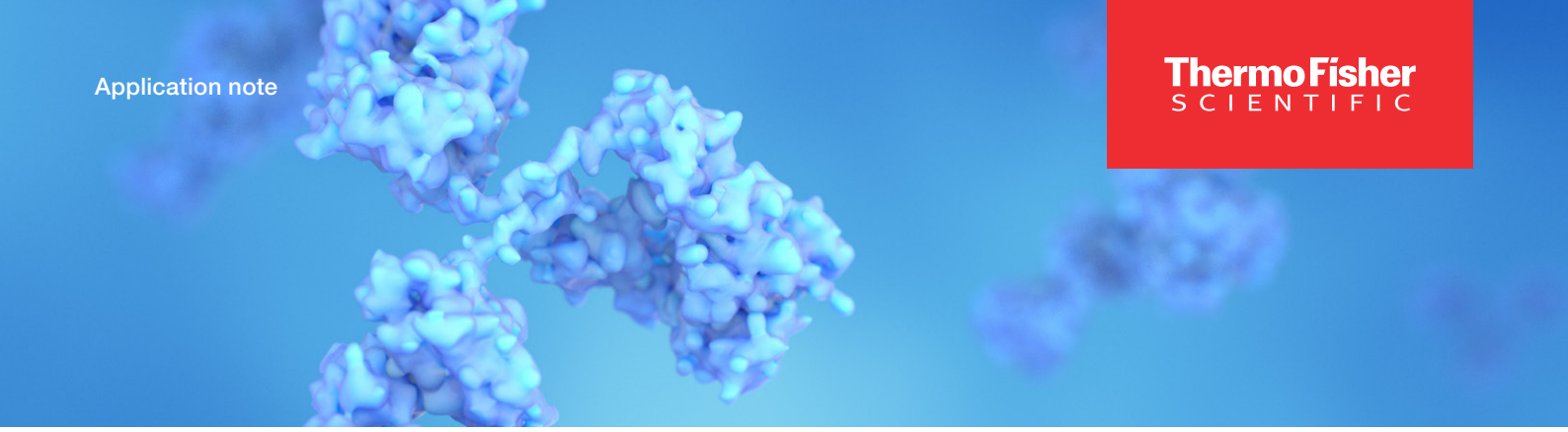

Quantify protein and peptide preparations at 205 nm

NanoDrop One Spectrophotometer

Figure 1. NanoDrop One Proteins Home screen showing available preprogrammed applications for protein quantitation.

Abstract

Life scientists can quantify peptide and protein samples on the Thermo Scientific™ NanoDrop™ One/One^{C} Microvolume UV-Vis Spectrophotometers using the A205 preprogrammed direct absorbance application. The new A205 application offers a choice of methods for peptides that contain Tryptophan and Tyrosine residues in their sequence as well as peptides that completely lack aromatic amino acids. The A205 application offers enhanced sensitivity for peptide quantification in seconds from only 2 µL of sample.

Introduction

Researchers have always needed ways to quickly quantify various biomolecules (e.g., protein and nucleic acid preparations) as a routine part of their workflows. This information helps them make informed decisions before proceeding with downstream experiments. There are many protein quantification methods to choose from including gravimetric approaches, colorimetric assays, direct spectrophotometric UV measurements (such as A280), and amino acid analysis. All of these methods have their strengths and weaknesses. Direct spectrophotometric microvolume UV measurements are a popular choice for researchers because they are simple to perform, require no reagents or standards, and consume very little sample. The NanoDrop One Spectrophotometer has preprogrammed applications (Figure 1) for direct quantification of proteins using absorbance measurements at 280 nm and 205 nm. This application note specifically describes how to use the Protein A205 application to quantify protein samples.

A protein's peptide backbone absorbs light in the deep UV region (190 nm-220 nm), and this absorbance can be used for protein sample quantitation. The A205 protein quantitation method has several advantages over the direct A280 protein method such as lower protein-to-protein variability (because A205 extinction coefficients are not based on amino acid composition) and higher sensitivity (because of the high molar absorptivity proteins have at 205 nm). However, technical limitations made it difficult to obtain these measurements in the past. Spectrometers' stray light performance, deep UV linearity, and protein buffers containing UV-absorbing components have all added to the challenge of obtaining A205 data. The NanoDrop One patented sample-rentention technology and low stray light performance have simplified quantification of small amounts of protein by A205 methods.

In this application note, we discuss the three A205 measurement options included in the NanoDrop One Protein A205 application and present performance data for each option.

A205 extinction coefficients for peptide and protein measurements

The NanoDrop One Protein A205 application allows customers to choose from three different options (Figure 2). The selected option will automatically determine the extinction coefficient that will be used to calculate the protein concentration based on the sample absorbance at 205 nm.

- ε_{205}=31 method
- Scopes method[2]
- Other = custom method $\varepsilon_{205}^{1mg/mL}$

Previous studies showed that most protein solutions at 1 mg/mL have extinction coefficients ($\varepsilon_{205}^{1mg/mL}$) ranging from 30 to 35[2]. The ε_{205} of 31 mL $mg^{-1}cm^{-1}$ is an extinction coefficient often used for peptides lacking tryptophan and tyrosine residues[1]. The Scopes method gives a more accurate ε_{205}, especially for proteins containing a significant amount of tryptophan (Trp) and tyrosine (Tyr) residues. The increased accuracy of this method takes into account the significant absorbance at 205 nm contributed by the aromatic side chains of Trp and Tyr. This method uses an A280/A205 ratio in its equation to correct for Trp and Tyr side-chain absorbance[3]. Recently, Anthis and Clore proposed the use of a sequence-specific ε_{205} calculation (e.g., custom/Other method), which is suitable for a wide range of proteins and peptides[1]. This method is appropriate for pure preparations of proteins or peptides whose amino acid sequences are known.

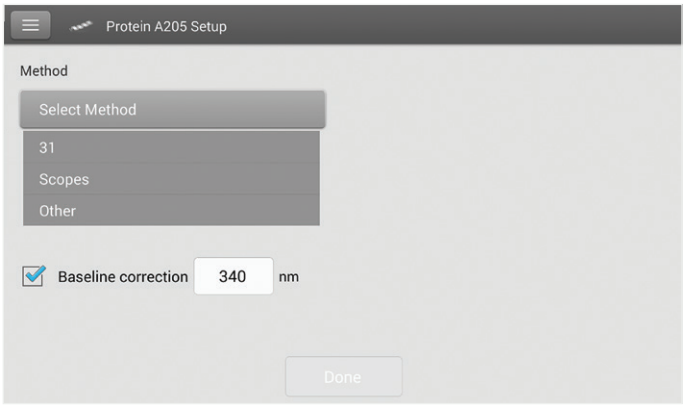

Figure 2. NanoDrop One Protein A205 methods selection screen.

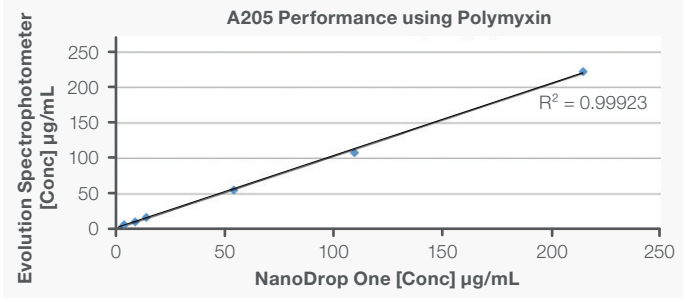

Figure 3. Polymyxin concentrations calculated with the Evolution Spectrophotometer and NanoDrop One instruments were plotted. Regression line shows that protein concentration measurements on the NanoDrop One instrument are in good agreement to those obtained on a traditional high end UV-Vis spectrophotometer.

A205 performance on the NanoDrop One

Preparations of polymyxin, a cationic detergent antibiotic with a peptide backbone, but no Trp or Tyr residues, were made in 0.01% Brij® 35 buffer and measured on the NanoDrop One and the Thermo Scientific™ Evolution™ UV-Vis Spectrophotometers. To ensure the validity of the measurements taken with the Evolution Spectrophotometer instrument, the polymyxin preparations were diluted in 0.01% Brij buffer to ensure that the measurements taken were within the linear range of the detector. For measurements on the NanoDrop One instrument 2 µL of sample were pipetted directly on the sample pedestal, while a 10 mm quartz cuvette was used for measurements on the Evolution Spectrophotometer. The polymyxin concentration data obtained on both instruments (Table 1) were plotted (Figure 3). Regression line shows that protein concentration results from the NanoDrop One instrument are in good agreement to the results obtained on a traditional high end UV-Vis spectrophotometer using a cuvette.

Target [Conc] mg/mL	NanoDrop One			Evolution
	A205	Std. Dev.	[Conc] mg/mL	[Conc] mg/mL
0	-0.01	0.04	-0.18	-0.02
5	0.11	0.01	3.60	5.05
10	0.27	0.01	8.84	10.53
15	0.44	0.02	14.08	17.09
50	1.68	0.01	54.14	55.32
100	3.39	0.01	109.44	108.48
200	6.64	0.03	214.16	222.50

Table 1. Various preparations of Polymyxin were measured on the NanoDrop One and Evolution Spectrophotometers. Five(5) replicates of each solution were measured on the NanoDrop One instrument using the 205=31 application. Solutions with absorbance over 1.0A were diluted and measured in triplicate on the Evolution Spectrophotometer instrument.

Protein Preparation	# of Trp of Tyr					
	Trp	Tyr	A205	STDV	[Concentration] ε_{205}=31 (µg/mL)	[Concentration] Scopes Method (µg/mL)
BSA 1	3	21	3.960	0.013	127.73	131.80
BSA 2	3	21	37.271	0.218	1202.30	1261.71
BSA 3	3	21	70.044	0.239	2259.48	2387.91
BSA 4	3	21	129.170	1.458	4166.77	4345.20
BSA 5	3	21	271.027	0.851	8742.81	9198.13
Lysozyme 1	6	3	29.069	0.169	937.71	795.95
Lysozyme 2	6	3	53.651	0.545	1730.68	1459.05
Lysozyme 3	6	3	102.713	0.668	3313.32	2814.79
Polymyxin 1	0	0	0.112	0.015	3.60	3.12
Polymyxin 2	0	0	0.274	0.014	8.84	10.12
Polymyxin 3	0	0	0.437	0.021	14.08	16.03
Polymyxin 4	0	0	1.678	0.014	54.14	60.99
Polymyxin 5	0	0	3.393	0.014	109.44	125.16
Polymyxin 6	0	0	6.639	0.034	214.16	244.87

Table 2. Comparison of different A205 methods for various protein and peptide preparations on the NanoDrop One Spectrophotometer.

To assess the effect that the extinction coefficients used at 205 nm (i.e., Scopes and ε_{205}=31 methods) would have on the result, we prepared dilutions of three different proteins with varied amounts of aromatic residues: bovine serum albumin (BSA, 3 Trp and 21 Tyr residues), lysozyme (6 Trp and 3 Tyr residues) and polymyxin (no Trp, no Tyr). These preparations were measured on the NanoDrop One instrument using the ε_{205}=31 and Scopes methods (Table 2).

Conclusion

To assess NanoDrop One Spectrophotometer performance at A205, we compared polymyxin concentration results obtained with the NanoDrop One and the Evolution benchtop Spectrophotometers, which have excellent stray light performance. Table 1 shows that the NanoDrop One instrument provided very consistent results between replicate measurements at 205 nm with standard deviations below 0.04A. In addition, the results obtained with both instruments were comparable (Figure 3). Comparison between the A205 methods (Scopes and ε_{205}=31 methods) offered in the NanoDrop One A205 application shows that the number of tryptophan and tyrosine residues has a large effect on the calculated concentration (Table 2). This is because tryptophan is the largest contributor to A280 absorbance, and the Scopes method uses the A280/A205 ratio to correct for aromatic side-chain absorbance at A205.

Our results show that A205 quantification using the ε_{205}=31 method gives comparable results when proteins have only a few tryptophan residues.

One limitation of the A205 method is that many of protein buffers commonly used have absorbance at 205 nm. Before using this technique, we recommend checking the protein buffer for any contribution to the absorbance at 205 nm.

References

1. Anthis, NJ and Clore, GM 2013. Sequence-specific determination of protein and peptide concentrations by absorbance at 205 nm. *Protein Science* 22:851-858.
2. Goldfarb, AR, Saidel, LJ, Mosovich E 1951. The ultraviolet absorption spectra of proteins. *Journal of Biological Chemistry* 193(1):397-404.
3. Scopes, RK 1974. Measurement of protein by spectrophotometry a 205 nm. *Analytical Biochemistry* 59:277-282.

Application note

Spectrophotometric Analysis of Ibuprofen According to USP and EP Monographs

Performing pharmaceutical identification tests with an Evolution UV-Visible Spectrophotometer

Introduction

Monographs outlined by the United States Pharmacopeia (USP) and European Pharmacopoeia (EP) contain tests, procedures, and acceptance criteria that help to ensure drug ingredients and drug products conform to the published requirements for strength, quality, and purity. These monographs contain detailed instructions utilizing a variety of analytical instrumentation for performing identification tests, purity tests, and tests to limit the amount of undesirable impurities. Although the general requirements governing the performance of an analytical instrument used in a monograph will be outlined in its own general chapter, additional instrument requirements needed to perform a test may be indicated in the individual monographs.

This document will highlight the utilization of UV-Visible spectrophotometers to perform essential monograph tests. As spectrophotometric tests are featured in hundreds of monographs, UV-Visible spectrophotometers are essential analytical instrumentation for every pharmaceutical quality control laboratory. In this work, a Thermo Scientific™ Evolution™ Pro using Thermo Scientific™ Insight™ Pro Software will be used to perform the USP and EP spectrophotometric identification tests for ibuprofen highlighted in their respective monographs.

Ibuprofen is an active pharmaceutical ingredient that is used as a medication for treating pain, fever, and inflammation. The Ibuprofen monographs published by USP and EP contain a variety of identification tests utilizing infrared absorption spectroscopy, ultraviolet visible spectroscopy, melting point analysis, and chromatography to help confirm the quality of ibuprofen samples.

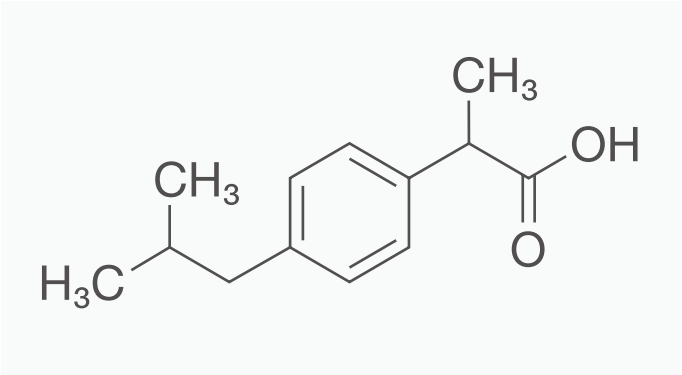

Figure 1. Chemical Structure of Ibuprofen, $C_{13}H_{18}O_2$.

Experimental

EP Identification Test

The spectrophotometric ibuprofen identification test according to the EP ibuprofen monograph requires measuring a test sample and comparing the ratios of its absorbance values to confirm they are within an acceptable range.

A 500 µg/mL ibuprofen solution was prepared by dissolving 50 mg in a solution of 0.1 M sodium hydroxide in a 100 mL volumetric flask using the sodium hydroxide solution to fill to the total volume. The sodium hydroxide solution was used as the blank. The monograph required a spectrum of the ibuprofen solution to be obtained with a wavelength range of 240 nm – 300 nm, a bandwidth of 1 nm, and a scan speed of less than or equal to 50 nm/min. The Insight Pro software experimental parameters used to obtain the spectrum are shown in Figure 2. The programed ratio equations for evaluating the results are shown in Figure 3.

Figure 2. Experimental parameters of EP ibuprofen test.

The spectrum of the ibuprofen test sample is shown in Figure 4. Visual inspection of the spectrum shows absorption maxima at 264 nm and 272 nm and a shoulder at 258 nm which align with the monograph requirement for the identification of ibuprofen.

Along with this spectrum, Insight Pro Software automatically calculates the ratio values required to verify the identity of ibuprofen using the programed equations from Figure 3. The absorbance ratio of A_{264}/A_{258} was 1.25 which was within the 1.20 – 1.30 requirement highlighted in the ibuprofen monograph. The Absorbance ratio of A_{272}/A_{258} gave a result of 1.00 which was also within the monograph requirement of 1.00 – 1.10. These absorbance ratios along with the visual inspection of the spectrum confirm the identity of ibuprofen according to the Ultraviolet and visual absorption spectrophotometry test in the EP ibuprofen monograph.

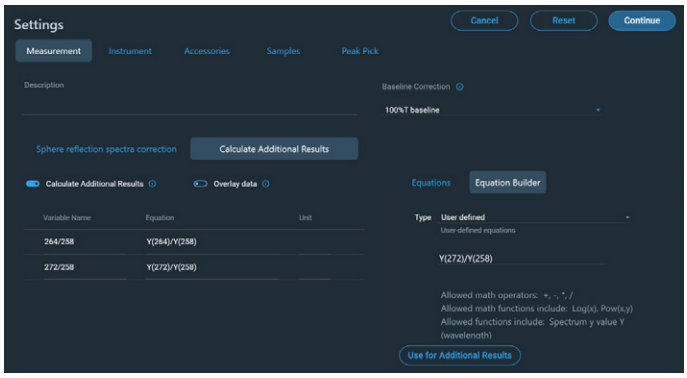

Figure 3. Ratio calculations for EP ibuprofen test.

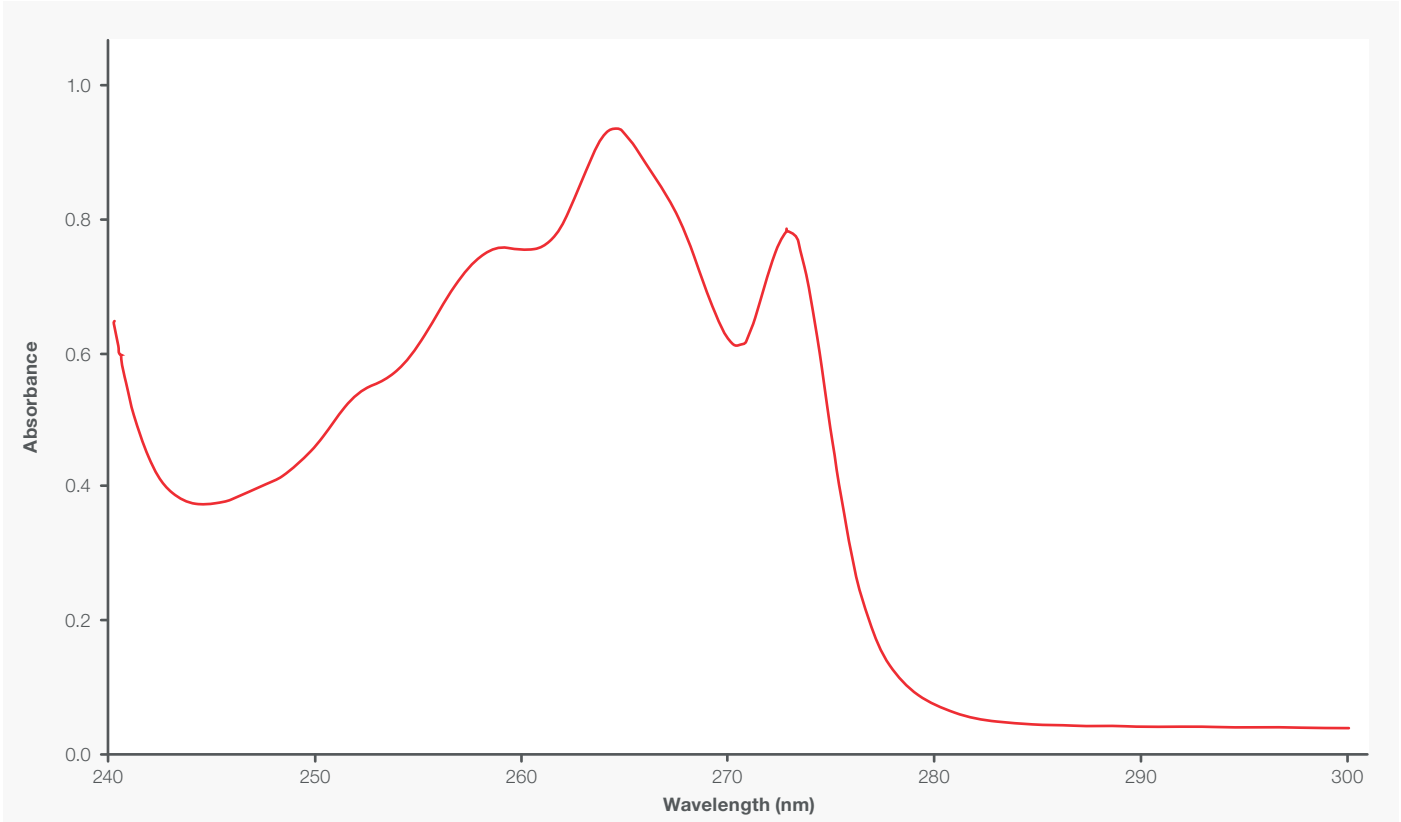

Figure 4. EP ibuprofen test sample spectrum.

USP Identification Test

In the USP spectrophotometric identification test for ibuprofen, a reference standard sample and a test sample are prepared using identical procedures and the spectra are compared to confirm the test sample exhibits absorption maxima and minima only at the same wavelengths as those of the reference sample. Additionally, the molar absorptivity at two different wavelengths are calculated and compared between reference standard and sample to ensure they do not differ within a certain percentage.

A 250 µg/mL solution of an ibuprofen standard was prepared by dissolving 25 mg in a solution of 0.1M sodium hydroxide in a 100 mL volumetric flask using the sodium hydroxide solution to fill to the total volume. A test ibuprofen solution was prepared in the same way as the standard. The sodium hydroxide solution was used as the blank in the experiment.

Spectral measurements of the reference standard and sample were obtained using a similar procedure as the EP Identification Test in Figure 2 but scanning from 200 nm – 400 nm. The spectral data should be similar to the results shown in Figure 4 with maxima and minima at the same wavelengths.

The absorbance values at 264 nm and 273 nm of both the standard and test solution were measured according to the USP guidelines using the Fixed method on the Evolution Pro Spectrophotometer with the following parameters as shown in Figure 5.

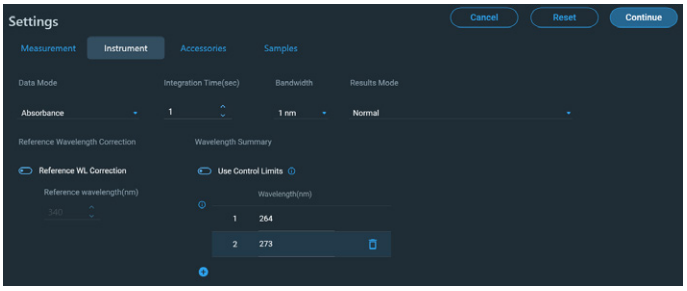

Figure 5. Experimental parameters of USP ibuprofen test.

	Weight (mg)	A_{264}	A_{273}	ε_{264}	ε_{273}
Standard	25.8	0.4732	0.3905	385.83	318.35
Sample	24.9	0.4644	0.3849	378.61	313.85

Table 1. USP Measurement Data.

The absorptivity values at each wavelength for both the standard and test sample were calculated using the Beer-Lambert Law where ε is the molar absorptivity in L/mol•cm units, A is the absorbance value, l is the pathlength in cm and c is the concentration in mol/L:

$$\varepsilon = \frac{A}{l \times c}$$

The molar absorptivity is calculated using the absorbance values and the weight of the samples. An example is shown below where the molar absorptivity of the standard sample at 264 nm was calculated as shown below:

$$\varepsilon = \frac{0.4732}{1 \text{ cm} \times 0.00122649 \text{ mol/L}}$$

$$\varepsilon = 385.83 \text{ L/mol}$$

The measured weight, absorbance at each wavelength, and calculated absorptivity at each wavelength for the reference standard and test sample are shown in Table 1.

The percent difference between the absorptivities of the sample and standard at both 264 nm and 273 nm were calculated using the following formula where the Average ε is the average of the Test ε and Standard ε at each respective wavelength:

$$\text{Percent Difference} = \frac{\text{Sample } \varepsilon - \text{Standard } \varepsilon}{\text{Average } \varepsilon} \times 100$$

Using this formula, we obtain a percent difference between the Standard and Sample of 1.9% for the 264 nm absorptivity and 1.4% for the 273 nm absorptivity. The USP test requires the difference between the respective absorptivities at 264 nm and 273 nm to be less than or equal to 3.0%. Since the test sample has a percent difference of less than 3.0% at both wavelengths, it meets the identification requirement in the ibuprofen USP monograph.

Conclusion

Spectrophotometers are utilized in hundreds of pharmaceutical monographs which make them essential instrumentation for confirming the identity of drug ingredients and drug products. The Thermo Scientific Evolution Series Spectrophotometers are ideal for performing these tests due to their versatility, ease of use, and superior performance. In this document both the USP and EP identification tests for each respective ibuprofen monograph was completed with an Evolution Pro Spectrophotometer. The identity of an ibuprofen test sample was confirmed according to the USP requirements when compared to a standard ibuprofen sample. The identity of an ibuprofen test sample was also confirmed according to the EP requirements through visual inspection and by comparing absorbance ratios.

References

1. United States Pharmacopeia and National Formulary (USP 43-NF 38), Monographs, Ibuprofen
2. European Pharmacopeia (EP 9.6), Monographs, Ibuprofen

Ordering information

Product	Part number
Evolution One UV-Vis Spectrophotometer	840-341400
Evolution One Plus UV-Vis Spectrophotometer	840-341500
Evolution Pro UV-Vis Spectrophotometer	840-340200

Learn more at **thermofisher.com/uv-vis**

thermo scientific

Application note

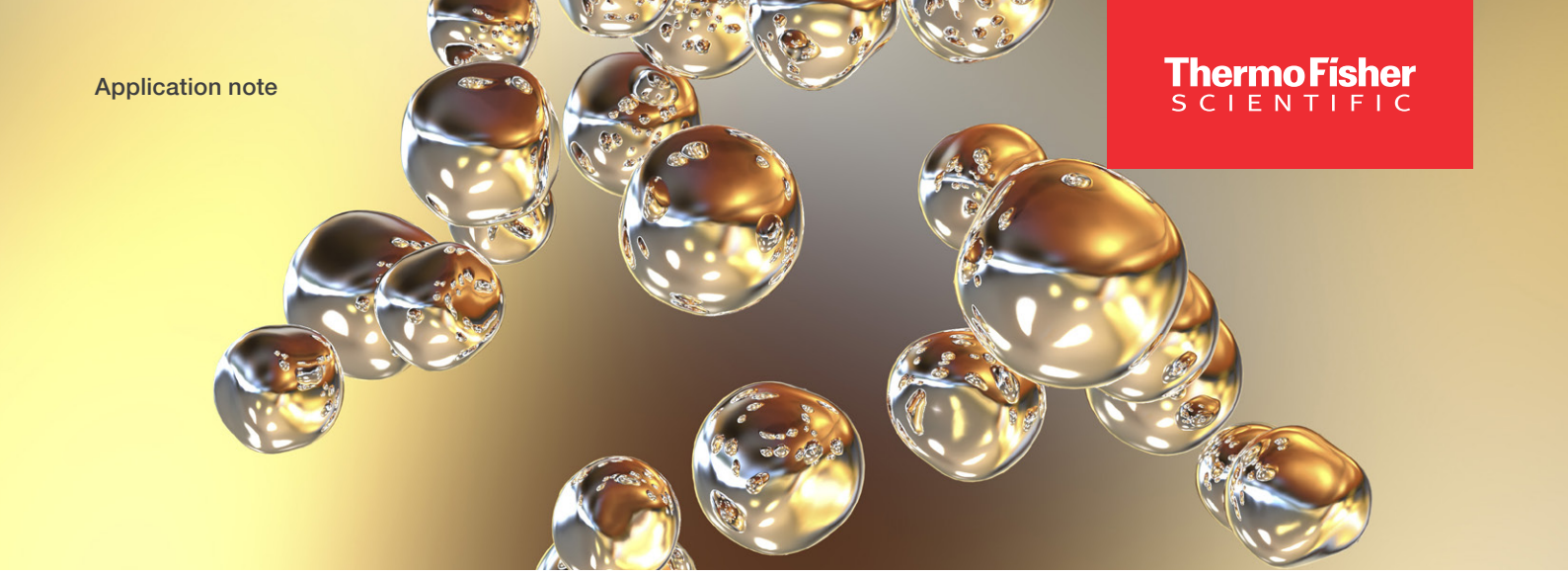

Observation of gold nanoshell plasmon resonance shifts after bioconjugation

Using the NanoDrop One Microvolume UV-Vis Spectrophotometer

Authors

Kejian Li[1], Megan N. Dang[1], Alexis B. Duffy[1] and Emily S. Day[1,2,3]

[1] University of Delaware, Dept. of Biomedical Engineering, Newark, DE, USA

[2] University of Delaware, Department of Materials Science and Engineering, Newark, DE, USA

[3] Helen F. Graham Cancer Center and Research Institute, Newark, DE, USA

RNA interference (RNAi)-based therapy has shown great potential in improving the study and treatment of diseases whose genetic underpinnings are known. However, challenges such as susceptibility to nuclease degradation, low cellular uptake, or rapid clearance from circulation impede the successful preclinical and clinical application of RNAi therapeutics.[1] To overcome these limitations, small interfering RNAs (siRNAs) or microRNAs (miRNAs) can be conjugated to nanoparticles (NPs), such as nanoshells (NS), to improve their stability, cellular uptake, and blood circulation time, thus resulting in increased effectiveness.[2, 3, 4]

Prior to using RNA-NP conjugates in therapeutic applications, it is critical to confirm successful RNA conjugation to the NP. One common method to confirm molecule loading onto gold-based NPs involves evaluating the surface plasmon resonance (SPR) spectra of the NPs before and after functionalization; successful RNA attachment will typically cause a slight red-shift in the peak SPR wavelength. Traditionally, UV-Vis spectrophotometers are used to analyze the optical properties of gold-based NPs. For example, the peak absorbance can be utilized to determine NP concentration via Beer's Law and to evaluate changes due to any surface modification. However, conventional cuvette-based UV-Vis spectrophotometers have limited linear range due to the use of a standard fixed pathlength (10 mm) cuvette, and they often require relatively large sample volumes (ranging from 0.5 mL to 3 mL). This is not ideal for conserving precious samples such as NPs coated with expensive RNA molecules. Furthermore, the need to dilute samples to fit the operating range of the instrument is time-consuming and increases the likelihood for inaccurate measurements. Alternative measurement techniques that require less volume and allow analysis of concentrated samples without dilution would be ideal.

Recent work has shown that the Thermo Scientific™ NanoDrop™ One Microvolume UV-Vis Spectrophotometer can be used to accurately measure highly concentrated NP samples without dilution, owing to its surface tension system and auto-ranging pathlength technique.[5, 6] For example, 150 nm diameter NS can be measured at concentrations up to 100 pM with high reproducibility.[5] In this application note, the use of the Nanodrop One instrument to observe shifts in the SPR of NS after conjugation to thiol-modified siRNA duplexes and

methoxy-poly(ethylene glycol)-thiol (mPEG-SH; a passivating agent) was investigated. The results indicate that the Nanodrop One instrument can serve as a microvolume alternative to traditional cuvette-based spectrophotometers for qualitatively confirming RNA and PEG loading on gold-based NPs via plasmon resonance shifts.

Experimental procedures

NS were synthesized by published protocols via the Oldenburg method.[7] First, 3-5 nm diameter gold colloid was made by the Duff method[8] from hydrogen tetrachloroaurate (III) hydrate (HAuCl4) (VWR), tetrakis(hydroxymethyl)phosphonium chloride (VWR), and 1 N sodium hydroxide (Fisher Scientific). The gold colloid was then combined with 120 nm diameter silica spheres functionalized with 3-aminopropyltriethoxysilane (Nanocomposix) and 1 M sodium chloride (NaCl) and rocked for 3-4 days at room temperature to create "seed" nanoparticles. The seed was purified twice via centrifugation at 3000 rpm for 30 minutes each and resuspended in Milli-Q® water (Sigma) to an optical density at 530 nm (OD530nm) of 0.1, as determined using a cuvette-based UV-Vis spectrophotometer. The diluted seed was mixed with additional HAuCl4 diluted in potassium chloride followed by addition of a small volume of 37% formaldehyde (VWR). The mixed solution was rapidly agitated to form complete gold shells and purified twice via centrifugation at 500 g for 15 minutes each. Additionally, NS were treated with 0.1% diethyl pyrocarbonate (DEPC) (Sigma) for 3 days rocking at 37°C to render the NS RNase-free. All materials described were purchased or treated with DEPC to be RNase-free prior to use.

siRNA oligonucleotides were purchased as single strands from IDT DNA, with sequences listed in **Table 1.** Thiolated sense strands were mixed with complementary non-thiolated antisense strands in equimolar amounts, boiled at 95° C for 5 min in a thermomixer, and then slowly cooled to 37° C over 1 hour to facilitate siRNA duplexing. RNase-free NS were diluted to OD800nm = 1.5 in Milli-Q water (as measured on a cuvette-based spectrophotometer). Next, 10% Tween-20 and 5 M NaCl were added to final concentrations of 0.2% and 12 mM, respectively, and the NS incubated for 5 min at room temperature. Then, siRNA duplexes were added to a final concentration of 200 nM, and the solution was bath sonicated and rocked at 4° C for 3 hours. NaCl was then added incrementally to a final concentration of 400 mM prior to rocking overnight at 4° C. The following day, 5 kDa mPEG-SH was diluted in Milli-Q water to 1 mM and added to NS to a final concentration of 10 µM. After rocking for 4 hours at 4° C, the NS solution was purified via centrifugation at 500 g for 5 minutes 3 times, resuspended in RNase-Free 1X phosphate buffered saline (PBS) with 100 X less volume of the starting NS, and stored at 4° C until use.

For conventional spectrophotometry, bare NS and siRNA-NS (diluted 100-fold in water) were placed in 1-cm pathlength disposable cuvettes and analyzed on a reference UV-Vis spectrophotometer from 1,100 nm to 400 nm. The NS concentrations were calculated from Beer's Law using the peak extinction (OD at ~800 nm) as determined by the spectrophotometer and the theoretical extinction coefficient of NS with 120 nm diameter silica cores and 15 nm thick gold shells. This revealed the initial bare NS and siRNA-NS had a concentration of 6.9 pM and 150 pM, respectively. To prepare samples for measurement with the NanoDrop One Spectrophotometer, the bare NS were concentrated by centrifugation at 500 g for 15 minutes, followed by removal of the supernatant and dilution in water to 100 pM. The siRNA-NS were directly diluted in water to 100 pM. The 100 pM bare NS and siRNA-NS solutions were measured on a NanoDrop One Spectrophotometer from 850 nm to 190 nm by pipetting 2 µL aliquots directly onto the sample pedestal. Between measurements, the NanoDrop One instrument sample pedestal was cleaned using a lint-free lab wipe. The auto pathlength option was turned on in the NanoDrop One Spectrophotometer software for each measurement.

Name	Sequence
siRNA sense	GCU GAU AUU GAC GGG CAG UAU / iSpPC//iSpPC//3ThioMC3-D/
siRNA antisense	AUA CUG CCC GUC AAU AUC AGC

Table 1: siRNA sense and antisense RNA sequences used in this work, denoted 5' to 3'. iSpPC is a photo-cleavable 10-atom spacer molecule, while 3ThioMC3-D is a thiol modification that facilitates attachment to gold NS.

Results

The absorption spectra of 150 nm NS, before (bare NS) and after (siRNA-NS) conjugation to thiolated siRNA and mPEG-SH at concentrations of 100 pM are shown in **Figure 1**. These spectra reveal the bare NS and siRNA-NS have a peak plasmon resonance at ~795 nm and ~804 nm, respectively, which is consistent with the spectra obtained using a reference spectrophotometer. The slightly red-shifted peak post functionalization, which maintains the overall shape and intensity of the spectra, provides evidence of successful siRNA and mPEG-SH conjugation. This was corroborated by dynamic light scattering and zeta potential measurements, as well as by siRNA loading quantification via OliGreen assay.[2, 4, 9] Notably, the spectra produced by the NanoDrop One Spectrophotometer were highly accurate and reproducible. Very little sample volume (2 µL) was used in the measurement, and no dilution was required for the analysis of highly concentrated samples (100 pM).

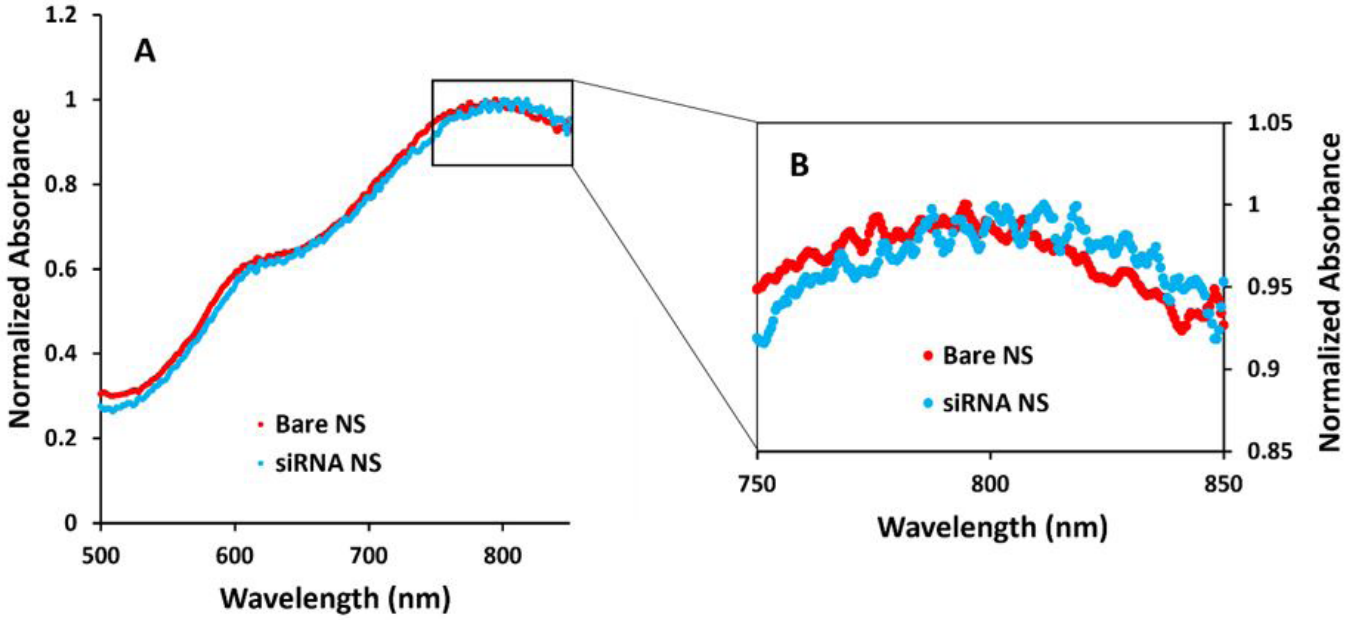

Figure 1: (A) UV-Vis spectra for Bare NS and siRNA-NS at concentrations of 100 pM, as measured on the NanoDrop One Spectrophotometer. n=3. (B) Zoom in of the UV-Vis spectra peak for Bare NS and siRNA-NS (750 nm to 850 nm).

Conclusions

This study demonstrates that the NanoDrop One Spectrophotometer can be used as a simple and reliable method to evaluate the surface modification of NS. The NanoDrop One Spectrophotometer can produce highly reliable results due to its built-in Thermo Scientific™ Acclaro™ Sample Intelligence Technology, which identifies common contaminants or other anomalies that may impact measurement accuracy. Additionally, the NanoDrop One Spectrophotometer allows the users to measure highly concentrated samples in 1–2 µL without dilution and produce full spectral data in seconds compared to a traditional cuvette-based spectrophotometer. These advantages save valuable time and money and help determine the quality and quantity of the sample before use in downstream applications. The ease of operation and small sample size requirement make the NanoDrop One Spectrophotometer an ideal and valuable instrument to characterize the properties of surface-modified NPs.

References

1. Wang, T.; Shigdar, S.; Shamaileh, H. A.; Gantier, M. P.; Yin, W.; Xiang, D.; Wang, L.; Zhou, S. F.; Hou, Y.; Wang, P.; et al. **Challenges and Opportunities for siRNA-Based Cancer Treatment.** *Cancer Lett.* 2017, 387, 77–83.
2. Riley, R. S.; Dang, M. N.; Billingsley, M. M.; Abraham, B.; Gundlach, L.; Day, E. S. **Evaluating the Mechanisms of Light-Triggered SiRNA Release from Nanoshells for Temporal Control Over Gene Regulation.** *Nano Lett.* 2018, 18, 3565–3570.
3. Artiga, Á.; Serrano-Sevilla, I.; De Matteis, L.; Mitchell, S. G.; De La Fuente, J. M. **Current status and future perspectives of gold nanoparticle vectors for siRNA delivery.** *J. Mater. Chem.* B 2019, 7, 876-896.
4. Dang, M. N.; Gomez Casas, C; Day, E. S. **Photoresponsive miR-34a/Nanoshell Conjugates Enable Light-Triggered Gene Regulation to Impair the Function of Triple-Negative Breast Cancer Cells**. *Nano Lett.* 2021, 21(1), 68-76.
5. Li, K.; Kapadia, C. H.; Dang, M. N.; Day, E. S. **Quantification of gold nanoshells using the NanoDrop One Microvolume UV-Vis Spectrophotometer.** https://www.thermofisher.com/document-connect/document-connect.html?url=https%3A%2F%2Fassets.thermofisher.com%2FTFS-Assets%2FMSD%2FApplication-Notes%2Fquantification-gold-nanoshells-nanodrop-one-uv-vis-spectrophotometer-an53464.pdf
6. Kapadia, C. H.; Melamed, J. R.; Day, E. S. **Quantification of gold nanoparticles using the NanoDrop One Microvolume UV-Vis Spectrophotometer.** http://assets.thermofisher.com/TFS-Assets/MSD/Application-Notes/AN53100-quantification-gold-nanoparticle.pdf
7. Oldenburg, S. J.; Averitt, R. D.; Westcott, S. L.; Halas, N. J. **Nanoengineering of optical resonances.** *Chem. Phys. Lett.* 1998, 288 (2–4), 243–247.
8. Duff, D. G.; Baiker, A.; Edwards, P. P. **A new hydrosol of gold clusters. 1. formation and particle size variation.** *Langmuir.* 1993, 9, 2301–2309.
9. Melamed, J. R.; Riley, R. S.; Valcourt, D. M.; Billingsley, M. M.; Kreuzberger, N. L.; Day, E. S. **Chapter 1: Quantification of siRNA duplexes Bound to Gold Nanoparticle Surfaces. In Biomedical Nanotechnology** *Humana Press*: New York, NY, USA, 2017.

Learn more at **thermofisher.com/nanodrop**

Color analysis for pharmaceutical products using UV-Visible absorption techniques

Introduction

The collection of reflected light by our eyes leads to the perception of an object's color, specifically light in the visible range of the electromagnetic spectrum (~400 nm – 700 nm). As our eyes are sensitive to variations in color and brightness,[1] small changes in the color of an object can be easily observed. In pharmaceutical manufacturing, the color of a drug product is important to analyze for QA/QC purposes. Not only is it necessary to minimize batch-to-batch variations for aesthetic purposes, but changes to the color of a product can have implications for the quality of the products. Specifically, variations from the anticipated color could indicate impurities are present in the product or that the material has degraded.[2–4] This is particularly important for materials which are easily decomposed, including light, moisture, and oxygen/air-sensitive substances.[5]

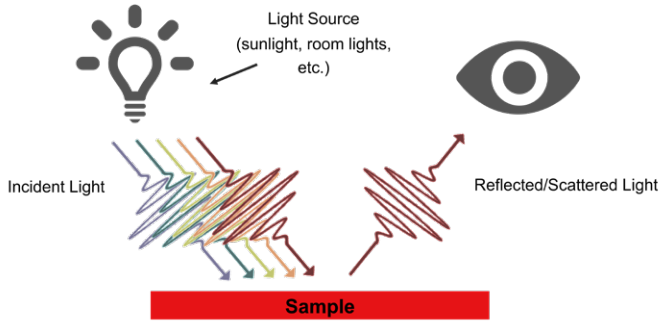

Figure 1: Diagram of how the color of an object is perceived.

Qualitatively, a comparison of the color of a finished drug product with an accepted standard can be used to ensure the material's color matches. However, inherently this methodology will introduce person-to-person variations.[6] Additionally, environmental effects, such as the light source or the presence of shadows, can influence the perceived color. As the color of a material comes from the reflected visible light, spectroscopic measurements of a material in the visible spectral range can be used to provide a more rigorous and quantitative method for assessing color. Consequently, a UV-Visible spectrophotometer can be used to measure either the percent of light transmitted (%T) or reflected (%R) across the visible spectrum for this purpose. As either of these measurement geometries can be used, this analysis can be applied to both liquid and solid products.

The American Society for Testing and Materials (ASTM),[7] as well as USP <1061>,[8] have detailed descriptions of the mathematics that can be used to assign the sample's color a coordinate in a graphical representation of color, also referred to as a color space. The tristimulus values, calculated through the equations 1 – 3,

$$X = \sum_{400}^{700} k * S(\lambda) * \bar{x}(\lambda) * R(\lambda)\Delta\lambda \quad (1)$$

$$Y = \sum_{400}^{700} k * S(\lambda) * \bar{y}(\lambda) * R(\lambda)\Delta\lambda \quad (2)$$

$$Z = \sum_{400}^{700} k * S(\lambda) * \bar{z}(\lambda) * R(\lambda)\Delta\lambda \quad (3)$$

are the basis of most other color spaces developed by the Comission Internationale de l'Eclairage (CIE).[9] These formulas include the measured reflectance ($R(\lambda)$), the spectral power of an illuminant ($S(\lambda)$), a color matching function ($\bar{x}(\lambda),\bar{y}(\lambda),\bar{z}(\lambda)$), and the normalization factor (k).

As described previously, the color of an object is highly dependent on environmental factors, such as light source and the field of view of the object. For example, the intensity of the light across the visible spectrum can be very different for various light sources and can lead to differences in how the color is observed. In the tristimulus equations, this factor is taken into account through the inclusion of the spectral power of the illuminant, $S(\lambda)$. A standardized intensity spectrum describing the spectral illuminant power as a function of wavelength was developed to describe a typical intensity spectrum for common illuminants (e.g., room lights, daylight), and is included in equations 1 – 3. Additionally, the observer angle, which defines the field of view of the material, can also alter the perceived color and is also accounted for in tristimulus equations through the color-matching functions.

The tristimulus values can condense the measured visible spectrum of a sample down to a single coordinate, however, the coordinate space is not uniform.[9] The lack of uniformity can lead to issues gauging the difference between the color of a sample and the color of a reference standard. In pharmaceutical applications, specifically in QA/QC functions, the ability to compare the sample to an accepted standard, as well as establish acceptance criteria, is critical. Consequently, a uniform color space must be used instead. CIE developed a set of mathematical functions which convert the calculated tristimulus coordinates into a uniform, cylindrical (CIE L*a*b*) or spherical (CIE L*C*h*) coordinate system (Figure 2), which is built on opposing color theory.

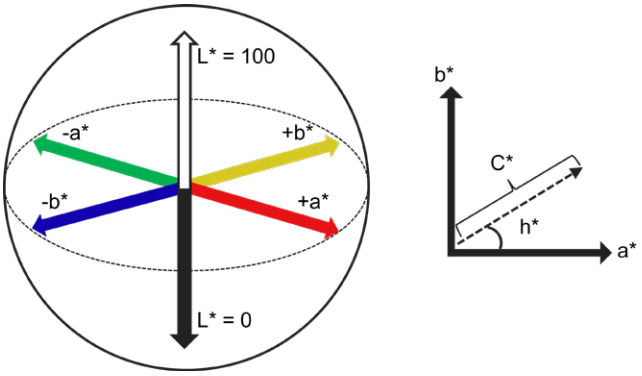

Figure 2: CIE L*a*b* and CIE L*C*h* coordinates

Coordinates for the more commonly used CIE L*a*b* color space are generated through the following mathematical functions,[7, 8]

$$L^* = 116\left(\frac{Y}{Y_n}\right)^{\frac{1}{3}} - 16 \quad (4)$$

$$a^* = 500\left[\left(\frac{X}{X_n}\right)^{\frac{1}{3}} - \left(\frac{Y}{Y_n}\right)^{\frac{1}{3}}\right] \quad (5)$$

$$b^* = 200\left[\left(\frac{Y}{Y_n}\right)^{\frac{1}{3}} - \left(\frac{Z}{Z_n}\right)^{\frac{1}{3}}\right] \quad (6)$$

where X, Y, and Z are the calculated tristimulus values and X_n, Y_n, and Z_n are the tristimulus values of a perfectly reflecting white diffuser. Here L^* describes how light (100) or dark (0) the materials are, a^* represents how red (positive) or green (negative) the sample is, and b^* demonstrates how yellow (positive) or blue (negative). As this transformation results in a more uniform color space, a better representation of the color difference (ΔE^*) between the sample and a standard can be developed. The color difference formula (eq 7) describes how a color difference is mathematically determined,

$$\Delta E^* = \sqrt{(L^*_{sam} - L^*_{std})^2 + (a^*_{sam} - a^*_{std})^2 + (b^*_{sam} - b^*_{std})^2} \quad (7)$$

where L^*_{sam}, a^*_{sam}, and b^*_{sam} represent the CIE L*a*b* values for the sample and L^*_{std}, a^*_{std}, and b^*_{std} represent the CIE L*a*b* values for the standard.[8] As a rule of thumb, two colors are considered to be indistinguishable from one another by eye if the color difference between the two substances is less than 3.

The CIE L*C*h* color space uses the same coordinate system as the CIE Lab system, except it reports the chroma (C_{ab}^*) and hue (h_{ab}^*) of the substance in place of a^* and b^*. Chroma is calculated through equation 8,

$$C^*_{ab} = \sqrt{a^{*2} + b^{*2}} \quad (8)$$

and describes how colorful a substance is wherein a small C_{ab}^* represents a more pale or muted color, while a large C_{ab}^* describes a substance with a very vibrant color. Hue describes the color of the object and is calculated through equation 9.

$$h^*_{ab} = \tan^{-1}\left(\frac{b^*}{a^*}\right) \quad (9)$$

Color analysis can be a quick and useful tool for assessing the overall quality of a given product prior to further downstream processing. Through UV-Visible absorption spectroscopy, the analysis can be made more rigorous, allowing for a more accurate measurement of color. Herein, we describe how color analysis can be applied to both solid and liquid samples using the Thermo Scientific™ Evolution™ Spectrophotometers and Thermo Scientific™ Insight™ Pro Software. Furthermore, descriptions of the USP requirements for color analysis of samples are explained in relation to the instrumental analysis method.

Thermo Scientific Evolution Spectrophotometers

Experimental

Materials

USP color-matching solutions were prepared based on descriptions in USP's chapter <631>,[10] which includes methods to analyze and report the color of solution phase samples. Briefly, three stock solutions were generated:

- 0.27 M $CoCl_2 \bullet 6H_2O$ (red solution)
- 0.17 M $FeCl_3 \bullet 5H_2O$ (yellow solution)
- 0.23 M $CuSO_4 \bullet 5H_2O$ (blue solution)

These solutions were mixed in different proportions to prepare the color-matching solutions A – T as defined in USP <631> (see Table 1).[10]

Table 1: Proportions of stock color solutions used to prepare color matching solutions A – T based on USP <631>.[10]

Color Matching Solution	Volume $CoCl_2 \bullet 6H_2O$ (mL)	Volume $FeCl_3 \bullet 5H_2O$ (mL)	Volume $CuSO_4 \bullet 5H_2O$ (mL)	Volume H_2O (mL)
A	0.1	0.4	0.1	4.4
B	0.3	0.9	0.3	3.5
C	0.1	0.6	0.1	4.2
D	0.3	0.6	0.4	3.7
E	0.4	1.2	0.3	3.1
F	0.	1.2	0.0	3.5
G	0.5	1.2	0.2	3.1
H	0.2	1.5	0.0	3.3
I	0.4	2.2	0.1	2.3
J	0.4	3.5	0.1	1.0
K	0.5	4.5	0.0	0.0
L	0.8	3.8	0.1	0.3
M	0.1	2.0	0.1	2.8
N	0.0	4.9	0.1	0.0
O	0.1	4.8	0.1	0.0
P	0.2	0.4	0.1	4.3
Q	0.2	0.3	0.1	4.4
R	0.3	0.4	0.2	4.1
S	0.2	0.1	0.0	4.7
T	0.5	0.5	0.4	3.6

For comparison against a more realistic example, two different cough syrups were analyzed. One sample was labeled "Daytime" and the other "Night-time." Additionally, a set of four antacid tablets of different colors were analyzed herein. The tablets were crushed into powders using a mortar and pestle.

Instrument parameters

UV-Visible measurements described herein were collected using an Evolution One Plus Spectrophotometer. For all samples, spectral measurements spanning 280 nm and 780 nm were collected using a 1.0 nm spectral bandwidth and 2 nm data interval.

The USP color-matching solutions were measured in transmission geometry and reported as % Transmission (%T), and the cough syrup samples were reported in absorption units. For both sample sets, deionized water was used to establish a 100% transmission baseline as the blank solution. All USP matching solutions were measured using a plastic 10 mm cuvette, while the cough syrup samples were measured in a 10 mm and 1 mm quartz cuvette.

The antacid samples were measured in reflection geometry using an integrating sphere accessory (ISA-220) with a powder cell holder. A white Spectrlon© disk was used to establish a 100% reflection baseline as the blank. The resulting data was reported as % Reflectance (%R).

Color analysis parameters

For all samples described herein, the CIE L*a*b* color values were calculated using Insight Pro Software. The D65 illuminant with a 10° observer angle was chosen to reflect the color of all samples. Color difference measurements were also performed through this software feature. All calculations performed correspond to the descriptions outlined in USP <1061>[8] and ASTM-E308.[7]

Results and discussion

Analysis of liquid samples—color matching solutions

According to USP <631>, color-matching solutions are to be used as a comparison point against the produced liquid product to ensure the product matches the expected color. As many liquid-based pharmaceutical products are yellow in hue, the USP monograph includes a procedure for making a set of standard solutions of varying yellow (Figure 3d).[10] EP has a different procedure outlined for making color standards and includes a wider range of colors, including brown, green and blue, among others.[11]

As shown in Figure 3d, some samples appear by eye to be similar and almost indistinguishable in color. However, as the purpose of these standards is to serve as different matching solutions, the variations in the color may be slight and difficult to compare without instrumental methods like UV-Visible color analysis. To demonstrate this concept, the percent transmittance of each matching solution was collected and are shown in Figures 3a – 3c.

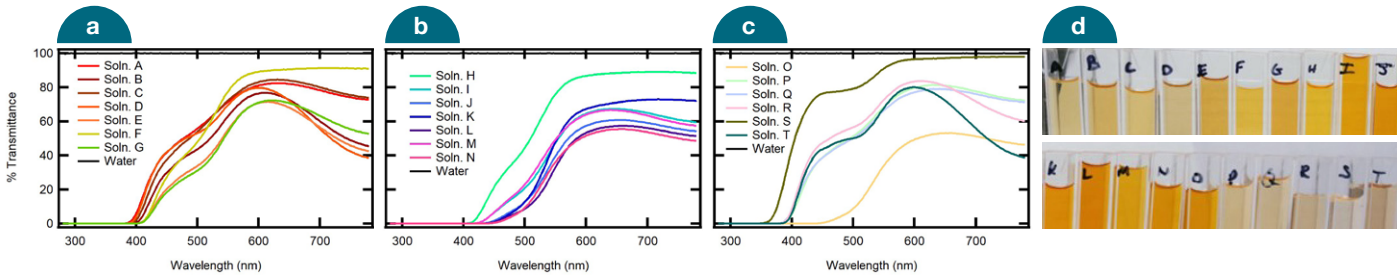

Figure 3: Absorption spectra of USP color matching solutions (a) A – G, (b) H – N, (c) O – T. (d) An image of the USP color matching solutions.

From these spectra, it is clear there are small differences in the transmittance, and consequently absorption, of each matching solution; however, color difference calculations were needed to rigorously compare the colors. As described previously, the CIE L*a*b* values were calculated using the Insight Pro Software. A select set of color-matching standards were chosen for comparison and are included in Table 2 as these standards (Soln. A and B, Soln. J and K, and Soln. Q and R) appear similar enough to each other in color that they are difficult to tell apart.

Table 2: CIE Lab and color difference values for select USP color matching solutions (A, B, J, K, Q, R). Color difference calculations were carried out for samples which appear similar by eye.

Solution	*L**	*a**	*b**	*ΔE**
A	87.5	0.5	28.5	**9.7**
B	83.3	2.4	37.0	
J	69.1	12.0	80.0	**12.5**
K	73.9	12.5	91.5	
Q	85.1	2.6	28.3	**5.2**
R	88.1	2.5	24.0	

The color difference values calculated between matching solutions A and B, J and K, and Q and R are relatively low; however, a numerical limit is required to put these difference values into context. In the pharmaceutical industry, different formulations may require different methods of comparison against a color-matching standard. For example, one product may need to have no discernable color (achromatic), while another must meet a minimum color value. Consequently, USP has developed a set of criteria which can be used to set acceptable limits for the calculated color difference from a standard (Table 3).

There are four main test limits which can be used depending on the color expectations for the analyzed product. Each test defines a limit to an acceptable color difference between the material and a given standard. For a sample which should have no color, the first test in Table 3 (colorless/achromatic) defines the necessary color difference limit as $\Delta E^* < 1$, where the color-matching standard is purified water.

For samples where the sample has an expected color, there are a few different options for analysis. If the color must match a given standard color exactly, the second test in Table 3 (Indiscernible from Standard) is required. Here, the color difference between the product and the color matching standard is used and must be less than 3. As mentioned previously, this defines the color difference that is discernable by the human eye.[10] The last two analyses define maximum and minimum color limits. Here, a sample can either be more or less colorful than a given standard. USP defines $\Delta h_{ab}{}^*$, the difference in hue between the sample and matching standard chosen must be less than 15. When setting the maximum or minimum color limit, instead of comparing the color difference against a number, two different analyses are required: one where the color of the standard is compared to the color of pure water ($\Delta E_{std}{}^*$) and one where the color of the product is compared against pure water (ΔE^*).

Table 3: Passing criteria for color difference tests from USP <631>.[10] For the maximum and minimum color difference measurements, $\Delta E_{std}{}^*$ refers to the color difference between a matching standard and purified water while ΔE^* refers to the color difference of the sample against purified water.

	Test	Color Standard	Passing Criteria
1	Colorless (Achromatic)	Purified Water	$\Delta E^* < 1$
2	Indiscernible from Standard	Color Matching Solution	$\Delta E^* < 3$
3	Maximum Color	Purified Water	$\Delta E^* < \Delta E_{std}{}^*$
4	Minimum Color	Purified Water	$\Delta E^* > \Delta E_{std}{}^*$

As the color difference values shown in Table 2 are intended to determine how similar the color of the two solutions are to one another, this analysis would follow the “Indiscernible from Standard” test. The passing criteria would require a calculated color difference of less than 3. For each set of standards, the color difference exceeds this limit, indicating they fail this test and are distinguishable from one another. This result highlights how small differences in color can be analyzed through the instrumental method, where it is difficult to perceive visually.

Analysis of liquid samples—cough syrup

The color-matching standards are ideal solutions with optimized component concentrations to produce a measurable spectrum in a standard 10 mm cuvette. Real samples may not be manufactured to produce UV-Visible absorption spectra that can be easily measured under these conditions. For example, Figure 4a includes the absorption spectra of a “Daytime” and “Night-time” cough syrup measured in a 10 mm cuvette. By eye, the “Daytime” syrup appears orange while the “Night-time” syrup appears red/purple.

As shown, both samples absorb greatly at wavelengths shorter than 550 nm (A > 3). In UV-Visible absorption measurements, it is good practice not to use highly absorptive samples for calculations or quantification, as very little light is allowed to pass through the sample and be detected by the system. For example, an absorption of 3 indicates 99.9% of the incident light is absorbed by the sample, leaving 0.1% of the light collected by the detector. Consequently, the absorption spectra in Figure 4a are not ideal for color analysis and result in the values described in Table 4.

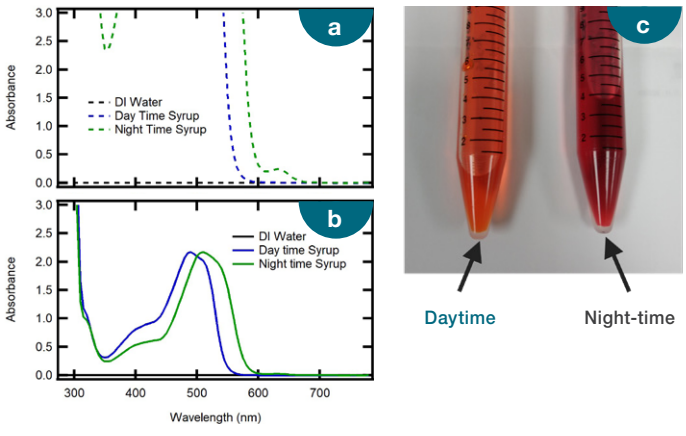

Figure 4: Absorption spectra of "Daytime" and "Night-time" cough syrup collected using a (a) 10 mm and (b) 1 mm quartz cuvette. (c) An image of the "Daytime" and "Night-time" cought syrup).

Table 4: CIE L*a*b* values for "Daytime" and "Night-time" cough syrup samples. Spectra were measured using a 10 mm and 1 mm path length.

	*L**		*a**		*b**	
Sample	10 mm cuvette	1 mm cuvette	10 mm cuvette	1 mm cuvette	10 mm cuvette	1 mm cuvette
Daytime	67.5	79.7	62.0	40.3	116.2	86.0
Night-time	40.2	62.3	68.5	72.2	69.2	27.6

To avoid issues for highly absorptive samples, instead a short pathlength cuvette can be used as absorption is directly proportional to pathlength according to Beer's law (eq. 10),

$$A = cl\varepsilon \quad (10)$$

where A is the collected absorbance, *c* is the concentration of the analyte, *l* is the path length, and ε is the molar absorptivity of the analyte. Changing the path length also circumvents the need to dilute the sample, avoiding some waste of the material.

Herein, both cough syrup samples were measured using a 1 mm cuvette, resulting in the absorption spectra in Figure 4b. Compared to the spectra shown in Figure 4c, the spectra collected show much more clearly the absorption features present in the sample. Included in Table 4 are the resulting color values based on the spectra collected with a shorter path length. These reported values are very different from the values calculated using the spectra collected with a longer path length. It is important to note that changing the path length not only changed the perceived lightness/darkness of the sample (*L**), but also how red/green (*a**) and how blue/yellow (*b**) the samples appear. This observation further illustrates the importance of measuring highly absorptive samples in a shorter path length to avoid significant deviations in the calculated color values. As good practice, quantification should only be performed when the highest peak absorption in the spectral region of interest is 1 A or lower. Given the calculated color values will be sensitive to the chosen path length, it is important any standard used for color difference calculations be measured using the same path length.

Analysis of solid samples

USP <631> specifically refers to color analysis procedures for liquids; however, color analysis can be performed using solid samples as well, according to USP <1061>.[8,11] For pharmaceutical analysis, the color of a solid drug product can also have implications on the quality of the material,[3–6] as described previously; however, it can also be used to indicate the dosage of a given product as well as comply with a company's branding or marketing needs.[6] For solid materials, measurements in reflection geometry are appropriate as it is difficult to pass light through a solid material without scattering effects. As described in equations 1 – 3, the tristimulus values, and therefore the CIE L*a*b* values, can be calculated using reflectance data, allowing for color analysis of solid samples.

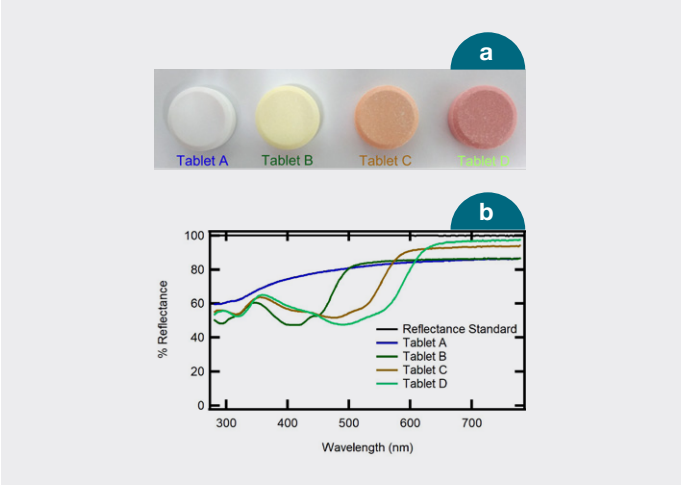

Figure 5 – (a) An image of the four antacid tablets measured. (b) Reflectance spectra of four antacid tablets (blue—Tablet A, dark green—Tablet B, brown—Tablet C, and light green—Tablet D) and a white reflectance standard (Spectralon).

Figure 5b includes the percent reflectance spectra (%R) of four antacid tablets (Fig. 3a) of varying colors. By eye, Tablets A – D appear white, yellow, orange, and red, respectively. The calculated CIE L*a*b* values for each sample are included in Table 5, along with the color values for a white Spectralon® reference material (99% reflectance). Color difference calculations were then performed to determine how different each antacid tablet was from the white reference material. Tablets B – D resulted in very high color differences (between 23 and 27) with respect to the reference standard, as anticipated as these samples are visually very different from the white standard. Tablet A, which appears white by eye, is closer in color to the reference, with a color difference of 8.7 compared with the color difference of the other three tablets, however as the calculated color difference is greater than 3, it is distinguishable from the reference standard and would fail a color matching test.

Table 5: Calculated CIE L*a*b* color values and color difference values for antacid tablets. Color Difference Calculations were carried out using the color values for the Spectralon® reference as the standard.

Sample	*L**	*a**	*b**	*ΔE**
Spectralon® Reference	100.0	0.0	0.0	—
Tablet A	92.8	0.3	3.4	7.92
Tablet B	92.8	-5.8	21.7	23.6
Tablet C	88.1	13.7	17.0	24.9
Tablet D	82.5	19.3	8.7	27.5

Conclusion

Color analysis can be an effective and quick method for QA/QC in pharmaceutical manufacturing. As shown in the experiments described herein, color analysis can be performed using the Evolution UV-Visible Spectrophotometers to carefully determine a material's color without person-to-person variations, allowing for a quantitative analysis of a produced pharmaceutical. Additionally, these measurements demonstrate the ability to analyze both liquid and solid samples following USP color analysis procedures.

References

1. Ng, S.E., Tay, Y.B.; Ho, T.Y.K.; Ankit; Mathews, N., Inorganic Electrochromic Transistors as Environmentally Adaptable Photodetectors, *Nano Energy*, **2022**, 97, 107142.
2. Zhou, L.; Vogt, F. G.; Overstreet, P. -A.; Dougherty, J. T.; Clawson, J. S.; Kord, A. S., A Systematic Method Development Strategy for Quantitative Color Measurement in Drug Substances, Starting Materials, and Synthetic Intermediates, *J. Pharm. Innov.*, **2011**, 6, 217 – 231.
3. Yamazaki, N.; Taya, K.; Shimokawa, K.-I., Ishii, F., The Most Appropriate Storage Method in Unit-Dose Package and Correlation between Color Change and Decomposition Rate of Aspirin Tablets, *Int. J. Pharm.*, **2010**, 396, 105 – 110.
4. Oram, P. D.; Strine, J., Color Measurement of a Solid Active Pharmaceutical Ingredient as an Aid to Identifying Key Process Parameters, *J. Pharm. Biomed. Anal.*, **2006**, 40, 1021 – 1024.
5. Berberich, J., Dee, K.-H., Hayauchi, Y., Pörtner, C., A New Method to Determine Discoloration Kinetics of Uncoated White Tablets Occurring During Stability Testing – An Application of Instrumental Color Measurements in the Development Pharmaceutics, *Int. J. Pharm.*, **2002**, 234, 55 – 66.
6. Hetrick, E. M.; Vannoy, J.; Montgomery, L. L.; Pack, B. W., Integrating Tristimulus Colorimetry into Pharmaceutical Development for Color Selection and Physical Appearance Control: A Quality-by-Design Approach, *J. Pharm. Sci.*, **2013**, 102, 2608 – 2621.
7. ASTM International. *Standard Practice for Computing the Color of Objects by Using the CIE System*; ASTM E308-08; West Conshohocken, PA.
8. United States Pharmacopeia and National Formulary. <1061> Color – Instrumental Measurement. In: USP–NF. Rockville, MD: USP
9. Subert, J.; Cizmarik, J., Application of Instrumental Colour Measurements in Development and Quality Control of Drugs and Pharmaceutical Excipients, *Pharmazie*, **2008**, 63, 331 – 336.
10. United States Pharmacopeia and National Formulary. <631> Color and Achromicity. In: USP–NF. Rockville, MD: USP.
11. European Pharmacopoeia. 2.2.2. Degree of Coloration of Liquids. In: European Pharmacopoeia. Strasbourg, France: European Pharmacopoeia.

Learn more at **thermofisher.com/evolution**

The NanoDrop Eight Spectrophotometer detects contaminating nucleic acids in mammalian DNA and RNA preparations

Introduction

Understanding nucleic acid sample quality and quantity is integral for many life science applications, reducing the occurrence of costly delays caused by troubleshooting downstream experimental failures. The Thermo Scientific™ NanoDrop™ Eight Microvolume UV-Vis Spectrophotometer measures eight samples at a time and provides you the ability to measure the concentration of biomolecules for high-throughput assays using a 1–2 µL sample size without the need for dilutions. With a measurement time of less than 20 seconds, you can easily insert the NanoDrop Eight Spectrophotometer into your high-throughput workflows.

The Thermo Scientific Acclaro™ Sample Intelligence Technology integrated within the NanoDrop Eight Spectrophotometer's software utilizes chemometrics to detect RNA in dsDNA sample preparations and dsDNA in RNA preparations to then calculate a corrected dsDNA or RNA concentration, respectively. Historically, the A260/A280 purity ratio has been utilized to assess nucleic acid sample purity; however, nucleic acid contaminants at low concentrations, such as RNA contamination in dsDNA samples, have a negligible effect on the purity ratio, and the contaminant identity is not easily determined by a change in the A260/A280 purity ratio or by visualizing the UV-Vis spectrum. Acclaro Technology's contaminant analysis capability eliminates the need for purity ratio assumptions and reports the contaminant present, contaminant absorbance, and a corrected sample concentration (Figure 1).

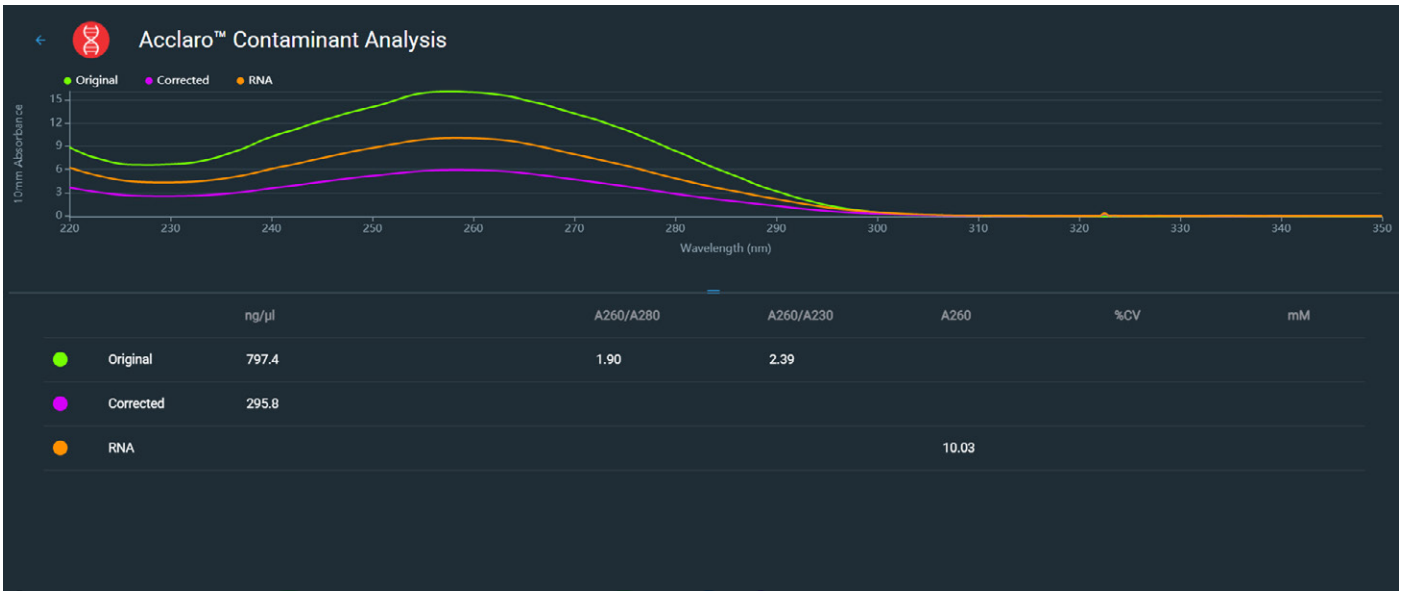

Figure 1: Acclaro Technology's contaminant analysis screen outlining the original concentration, corrected dsDNA concentration, and the absorbance contribution of RNA contamination. The original spectrum is shown in green, the corrected spectrum in pink, and the contaminating RNA spectrum in orange.

Materials and methods

Total RNA and genomic DNA from mouse tissue (BioChain Institute Inc., R1334035-50 and D1334999-G01) and RNA and genomic DNA from the MCF-7 cell line (BioChain Institute Inc., R1255830-50 and D1255830) were dialyzed and diluted in tris-EDTA buffer (TE pH 8.0, Fisher Scientific, BP2473500) and made into various DNA/RNA mixtures according to percentage of absorbance contribution. Triplicates of each mixture were measured on the NanoDrop Eight Spectrophotometer using fresh 1.0 µL aliquots per replicate for the dsDNA and RNA applications.

The NanoDrop Eight Spectrophotometer's Acclaro Technology-corrected results from the mouse and MCF-7 DNA/RNA mixtures were compared with the theoretical concentration and the original, uncorrected concentration in Figures 2 and 3 using the dsDNA and RNA applications, respectively. Acclaro Technology calculated an original, uncorrected concentration and a corrected concentration based on a modified Beer's Law equation and the absorbance contribution at 260 nm.

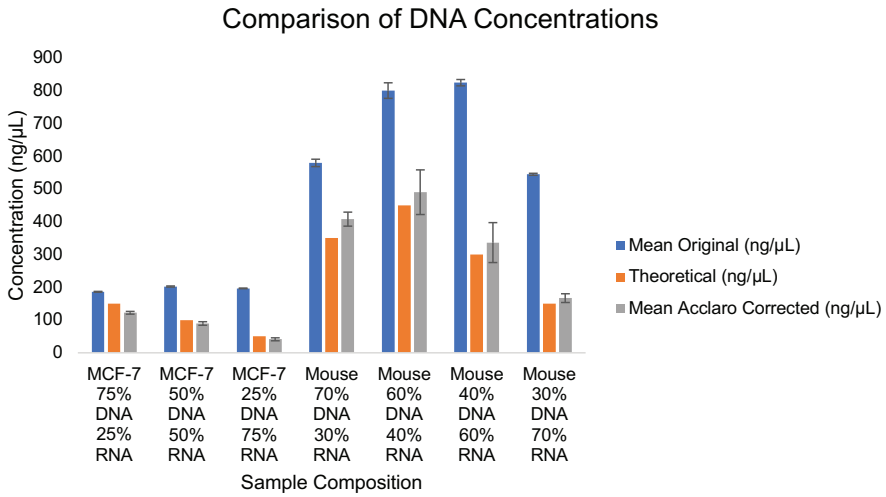

Figure 2: Comparison of the concentration reported by the Acclaro Technology for different sample compositions of DNA and RNA based on percentage of absorbance contribution. DNA and RNA from either the MCF-7 cell line or mouse tissue were mixed according to absorbance percentage and were measured using the dsDNA application. The mean original concentration (blue bars), the theoretical concentration (orange bars), and the mean Acclaro Technology software-corrected concentration (gray bars) were reported by the NanoDrop Eight Spectrophotometer's software. Error bars represent the standard deviation.

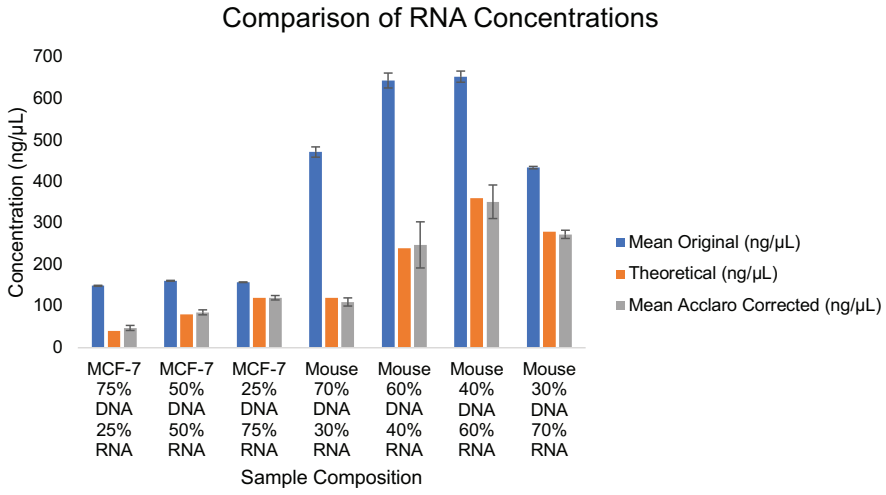

Figure 3: Comparison of the concentration reported by the Acclaro Technology for different sample compositions of DNA and RNA based on percentage of absorbance contribution. DNA and RNA from either the MCF-7 cell line or mouse tissue were mixed according to absorbance percentage and were measured using the RNA application. The mean original concentration (blue bars), the theoretical concentration (orange bars), and the mean Acclaro Technology software-corrected concentration (gray bars) were reported by the NanoDrop Eight Spectrophotometer's software. Error bars represent the standard deviation.

Results

In Figures 2 and 3, the Acclaro Technology's software-corrected mean concentration from the NanoDrop Eight Spectrophotometer was graphed against the original, uncorrected concentration and the theoretical concentration for the mouse and MCF-7 DNA/RNA mixtures with standard deviation shown as error bars. Since nucleic acids absorb at 260 nm, the original, uncorrected concentration is inflated compared to the Acclaro Technology's software-corrected concentration when DNA and RNA are both contributing to absorbance.

With the inclusion of the Acclaro Technology in the NanoDrop Eight Spectrophotometer's software, the corrected nucleic acid concentration was calculated after correcting for the contaminant absorbance contribution. This feature allows for simultaneous nucleic acid purity and quantity assessments. All the Acclaro Technology's software-corrected concentrations fall within ±20% of the theoretical concentration, with most samples within ±10%.

Conclusion

Contaminating nucleic acids in dsDNA or RNA preparations can cause costly delays in applications such as qPCR, where exact quantitation is crucial for a successful experiment. Since RNA and dsDNA both absorb at 260 nm, the true nucleic acid concentration will be overestimated with a copurified contaminant present. This overestimation can lead to experimental failures and require extensive troubleshooting. The ease with which the Acclaro Technology corrects for contaminating nucleic acids will save time, effort, and associated costs by improving sample purity and quantity assessments.

The function of the Acclaro Technology makes the nucleic acid purity assessment clear and simple. With each measurement of a nucleic acid sample, the NanoDrop Eight Spectrophotometer takes quality assessment a step further by outlining the contaminant identification, absorbance contribution, and the corrected sample concentration. The results from the experiments above indicate the NanoDrop Eight Spectrophotometer, which includes the Acclaro Technology in its software, can be implemented into many molecular biology workflows to obtain an accurate and advanced nucleic acid evaluation for downstream success.

Learn more at **thermofisher.com/nanodropeight**

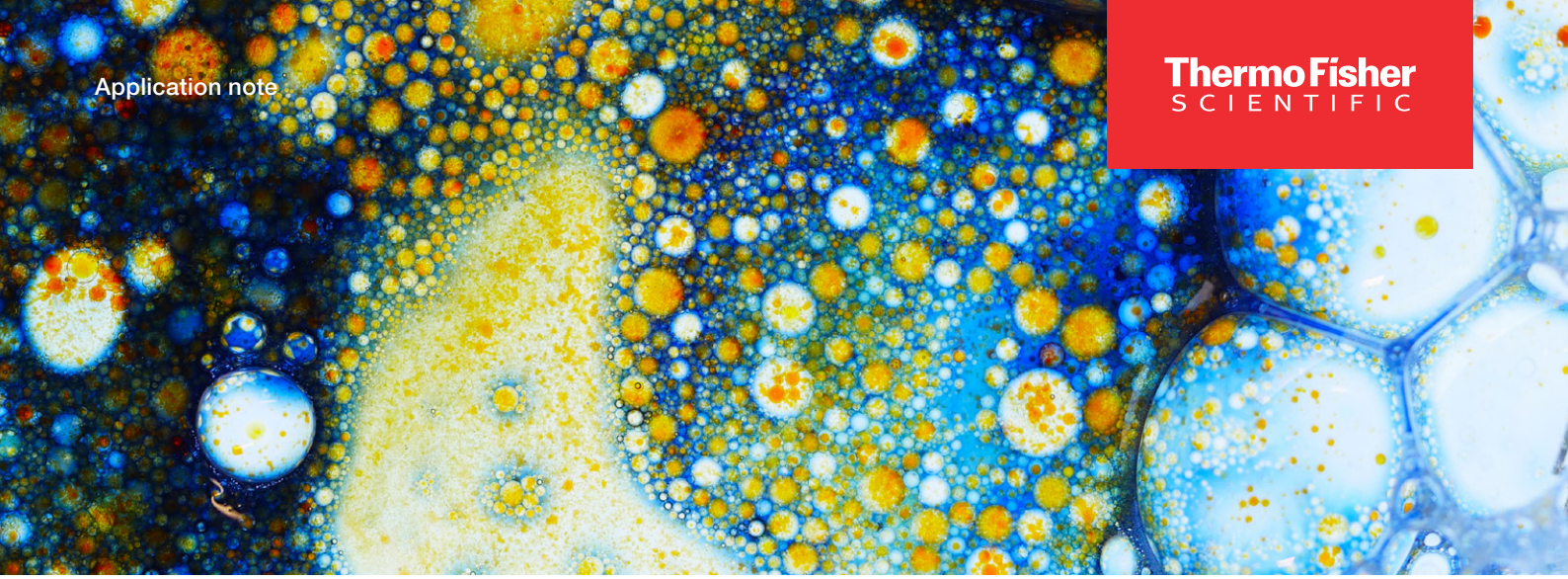

Application note

Enabling real-time release of final products in manufacturing of biologics

Authors

Shaileshkumar Karavadra,
David James, and Arnaud Di Bitetto,
Hemel Hempstead, UK

Keywords

DXR3 SmartRaman, spectrometer, biopharmaceutical, GMP, real-time release testing, QbD, RTRT, manufacturing, multi-attribute testing

Introduction

Biopharmaceuticals (or biologics) are manufactured using biological-expression systems (such as mammalian, bacterial, and insect cells) and have spawned a large and growing biopharmaceutical industry (BioPharmaceuticals). The structural and chemical complexity of biologics, combined with the intricacy of cell-based manufacturing, imposes a huge analytical burden to correctly characterize and quantify both processes (upstream) and products (downstream). In small-molecule manufacturing, advances in analytical and computational methods have been extensively exploited to generate process analytical technologies (PAT) that are now used for routine process control, leading to more efficient processes and safer medicines.

Raman spectroscopy is a vibrational spectroscopy technique with several useful properties (non-destructive, non-contact, high molecular-specificity, and robustness) that make it particularly suited for PAT applications in which molecular information (composition and variance) is required.

Typical good manufacturing practice (GMP) operations involve performing an extensive set of tests according to approved specifications before the material is released to the market or for further processing. Recent ICH guidelines (ICH Q8, Q9, Q10, and Q11), however, suggest an alternative real-time release strategy to provide assurance of product quality prior to release. Real-time release testing uses the principles of the pharmaceutical Quality by Design (QbD) to optimize release and stability testing. A combination of manufacturing process understanding, process control, and product knowledge can be used to demonstrate that the material was made according to GMP.

The exact approach to real-time release testing (RTRT) will vary depending on the process requirements. The RTRT strategy may be based on control of process parameters, monitoring of product attributes, or on a combination of both at appropriate steps throughout the process. Critically, the RTRT strategy should be based on a firm understanding of the process and the relationship between process parameters, in-process material attributes, and product attributes.

Quality, cost, and speed are the major drivers for implementing in-line monitoring, at-line monitoring, and real-time release.

Here, we review some of the most important applications of Raman spectroscopy to the manufacturing and analysis of biopharmaceuticals. This article covers two aspects of the biopharmaceutical-manufacturing process: identity/variance testing of raw materials and cell culture media; and multi-attribute product testing of a biologic drug product or final product testing of a biologic drug product.

Raw material characterization

Acceptance of raw materials today is often predicated on small-scale functional testing and/or limited analytical methods, which may not be representative of at-scale performance. This leads, in some cases, to fluctuating process outputs and, in extreme cases, not meeting predefined release criteria. Furthermore, many clinical products are developed using a small number of batches resulting in a narrow range of raw material variation and thus a limited process understanding. Especially in upstream cell culture, the unforeseen variability of various components of the cell culture media can impact a product's micro-heterogeneity and its critical quality attributes (CQA).

Multi-attribute tests for high-risk raw materials may include identity test, quantitative test for the concentration of key ingredients in a raw material, batch-to-batch variability test, and degradation tests.

One high-risk raw material encountered in biologics manufacturing is cell culture media. Identification of cell culture media samples by traditional liquid chromatography (LC) methods, such as amino acid or vitamin analysis, has high costs and requires significant analytical expertise and laboratory space. Raman spectroscopy offers many potential benefits, such as low cost, portability, and potentially limited skill required to operate the instruments.

Buffers are another set of critical raw materials used in downstream manufacturing. Osmolality is a measure of concentration and is considered a critical quality attribute and critical process parameter in bioprocessing. The yield and quality of a biologic are highly dependent on the optimization of the downstream process. Identity testing along with osmolality of buffers can be carried out using a multi-attribute method based on principal component analysis and partial list squares. Rapid testing of buffers through single-use flexi bags can be carried out using the fiber optics probe of the Thermo Scientific™ DXR3 SmartRaman Spectrometer at the point of use with no need for sample preparation.

Final product identity testing

Final product identification of biologics pre- and post-shipment is another regulatory requirement. Product testing for identity through different kinds of primary packaging (glass vials, syringes, glass bottles) poses a significant analytical challenge in the manufacturing of biologics. Fill finish sites may not have the necessary analytical expertise to carry out the tests and may have to send the samples to the parent site or external lab for testing, incurring time and money.

Moreover, biologics or small molecule drug products would also have to undergo retesting upon importation either from a third country in the EU member state or the USA when drug products have been sent to the USA from other countries. A full list of tests is typically carried out, including final product identity testing. For biopharma manufacturers, this involves either sending the samples back to the parent site for analysis or employing third-party labs in the country of import. This increases significant costs and delays in the delivery of highly needed drug products.

End product identity testing/final product identity testing of biologics after fill-finish or pre-shipping to the fill-finish line is carried out by a variety of analytical techniques depending on the molecule/registration dossier.

For example, the verification test for biologic proteins is peptide mapping—a long-established workflow for protein identification using LC/mass spectrography (MS). This complex separation technique requires protein extraction and clean-up, enzyme digestion, one or more stages of liquid chromatography, and two phases of mass spectrometry before the final spectrum is matched against protein databases. Although it is a standard methodology, peptide mapping necessitates an analytical lab with qualified technical resources, entails extensive time for preparation, and introduces significant costs in solvents, columns, and analytical equipment.

The DXR3 SmartRaman Spectrometer, with its high sensitivity and resolution, allows characterization of the drug product by evaluating the fingerprint region of the molecule. Therefore, the DXR3 SmartRaman Spectrometer's unique capability with sampling flexibility ensures repeatable measurements, and subsequent analysis allows rapid method development and deployment.

We ran a feasibility study for multinational drug manufacture whereby the primary goal was to set up a rapid multi-attribute end product test to differentiate 15 different types of drug products and determine the concentration of the two preservatives in the drug products.

For this feasibility test we were given 15 different types of biologic drug products that varied in concentration from 0.5 mg/mL to 6 mg/mL. Concentration of two preservatives A and B ranged from 0.85 mg/mL to 5.0 mg/mL and 0.42 mg/mL to 3.91 mg/mL respectively.

These commercial drug products were supplied in their native glass vials varying in size and volume. A picture of such glass vials is shown below (Figure 1).

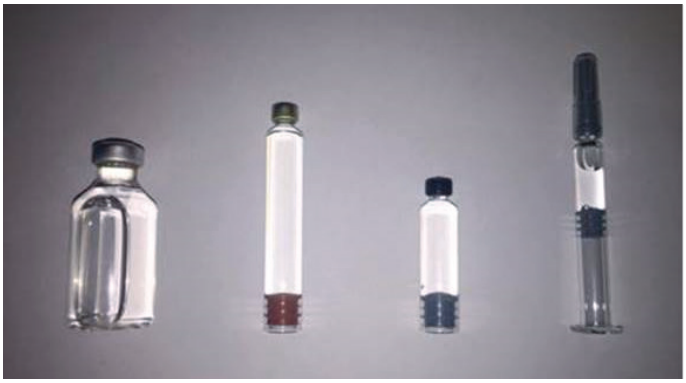

Figure 1. Typical native glass vials.

Reversed-phase high-performance liquid chromatography (HPLC) is currently used for the final product identity test and quantitative measurement of two preservatives in the final drug product.

DXR3 SmartRaman Spectrometer with universal sampling plate and 180-degree sampling module was used to acquire spectra of 15 drug products. To acquire each spectrum, a 532 nm laser with 40 mW power and 1 minute of scanning time was used. Ten spectra were acquired for each sample to accommodate the variability of glass vials and scattering effects.

DXR3 SmartRaman Spectrotometer offers excellent selectivity, repeatability, and full wavelength range to characterize biologics based on the characteristic band assignment (Table 1 and Figure 2).

Band frequency (cm^{-1})	Region	Vibrational mode	Protein structure assignments
870–1,150	Backbone, skeletal stretch	C_α-C, C_α-C_β, C_α-N	Secondary structure elements: α-helix, β-sheets, less-ordered structure
1,200–1,340	Amide III	N-H in-plane, Cα-N stretch	Hydrogen bonding, secondary structure
1,400–1,480	Side chain deformations	CH_2 and CH_3 deformations	Local environments, intermolecular interactions of side chains
1,510–1,580	Amide II	N-H deformations and C-N stretch (observed in UVRR and not conventional Raman spectra)	Local environments, intermolecular interactions of side chains
1,630–1,700	Amide I	C=0 stretch N-H in-plane bending	Secondary structure elements: α-helix, β-sheet, less-ordered structure

Table 1. Characteristic Raman band assignment.

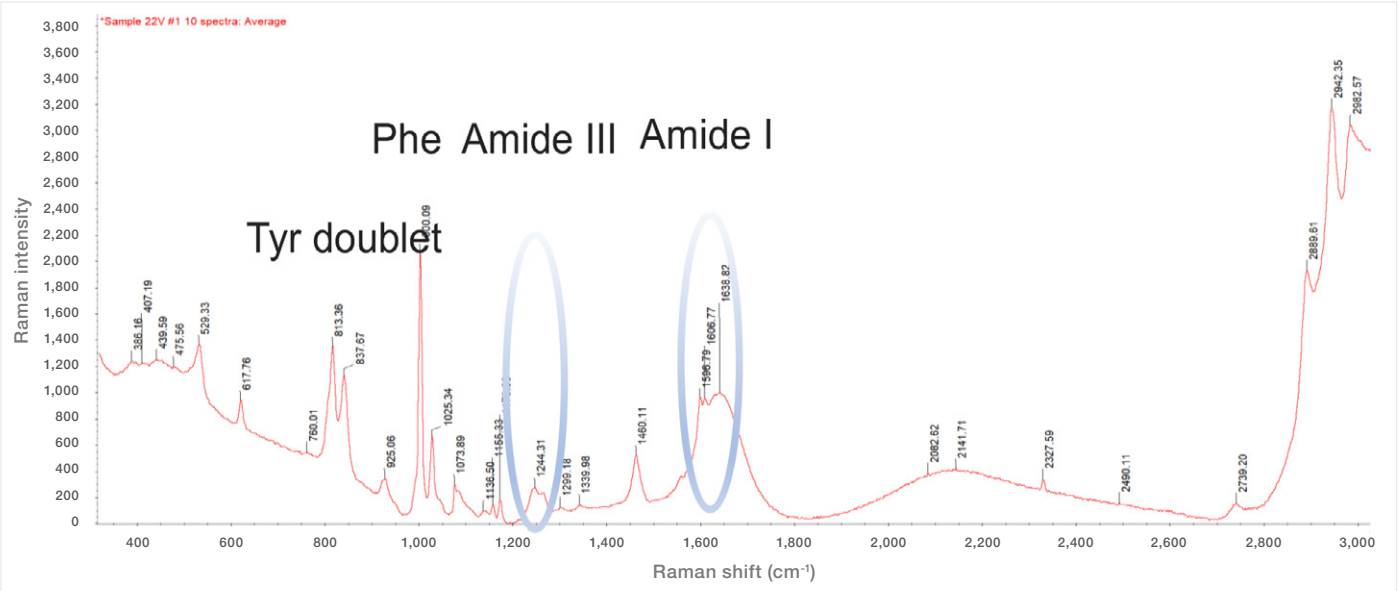

Figure 2. DXR3 SmartRaman spectrum showing characteristic bands of a biologic drug product.

Figure 3 shows the spectra of a sample containing a drug product against its placebo. It is imperative to establish that technique chosen for a feasibility study. In this case, Raman spectroscopy is sensitive enough to detect the differences between the drug product and its placebo. DXR3 SmartRaman Spectrometer offers high sensitivity to determine the significant differences between placebo and actual drug products.

Figure 4 is showing spectra of different classes of drug products. These spectra were utilized to build the discriminant analysis method on the Thermo Scientific™ TQ Analyst™ Software. TQ Analyst Software is a validated qualitative and quantitative method building software offering full compliance for pharmaceutical applications.

The discriminant analysis classification technique can be used to determine the class or classes of known materials that are most similar to an unknown material by computing the unknown's distance from each class center in Mahalanobis distance units. The discriminant analysis technique is typically used to screen incoming materials or final products to determine if they are compound/molecule a, b, or c.

Discriminant analysis methods typically specify at least two classes of known materials, but the method also works with only one class. Multiple standards may be used to describe each class (at least one class must contain two or more standards). Multiple regions of the spectrum may be used for the analysis.

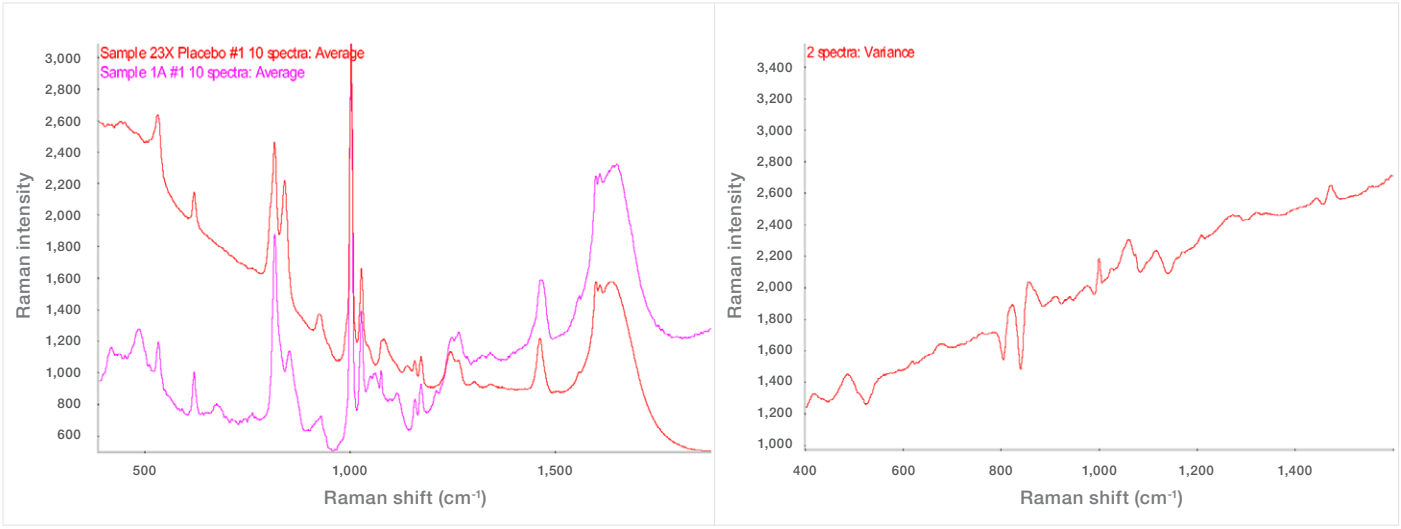

Figure 3. Raman spectra of drug product and its placebo and variance spectrum.

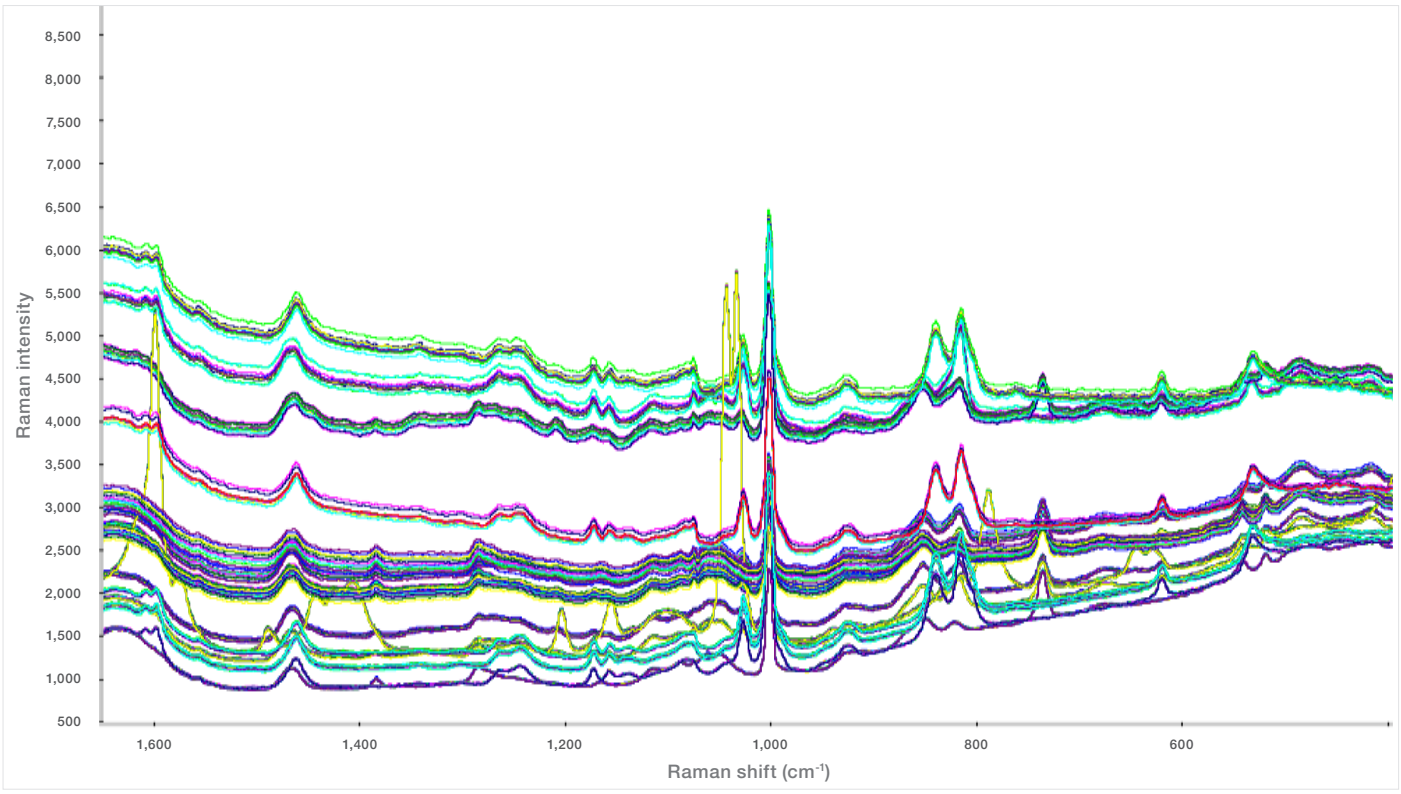

Figure 4. Raman spectra of different classes of drug products.

What does discriminant analysis do?

A discriminant analysis method applies the spectral information in the specified region or regions of an unknown sample spectrum to a stored calibration model to determine which class of standards is most similar to the unknown.

When the method is used to analyze an unknown sample or a class, the software performs a principal component analysis on the spectra of the standards and uses those results to determine score values for the unknown sample spectrum. The score plots are used to produce Mahalanobis distance values, which in turn are used to rank the classes.

The result of a discriminant analysis is the name of the class or classes that are most similar to the spectrum of the unknown sample. The Mahalanobis distance between the unknown sample and each reported class can also be reported. The closer each distance value is to zero, the better is the match.

After cross-validation, principal component scores plot revealed the class differentiation and the report indicated that all the classes of the different products were correctly identified with no mismatches to indicate false positives.

Quantitative analysis of biologics for preservative A and preservative B

As part of this feasibility study, our client also wanted to determine if the DXR3 SmartRaman Spectrometer test could be utilized to replace the HPLC test for measuring the concentration of two preservatives in their drug products. The level of preservative A was 0.85 mg/mL to 3.07 mg/mL and that of preservative B was 0.32 mg/mL to 2.57 mg/mL.

Pure samples of preservatives A and B were acquired as references, and to ascertain their presence in the final drug formulation.

Actual class	Mismatch	Calculated class	Calculated distance	Next class	Next distance
Product D		Product D	0.5809	C	4.5556
Product A		Product A	1.9869	I	12.9617
Product B		Product B	1.3796	E	25.1324
Product C		Product C	0.5417	D	3.8568
Product D		Product D	0.8466	M	9.0495
Product I		Product I	1.7709	A	13.9064
Product M		Product M	0.5284	S	3.3881
Product O		Product O	0.2244	X	17.3044
Product R		Product R	0.5419	C	4.4691
Product T		Product T	0.5944	X	2.3213
Product X		Product X	0.79	T	3.1646
Product S		Product S	1.1837	M	3.0829
Product N		Product N	1.0954	U	15.1798
Product U		Product U	0.1603	T	9.1738
Product S		Product S	1.8544	N	22.1624

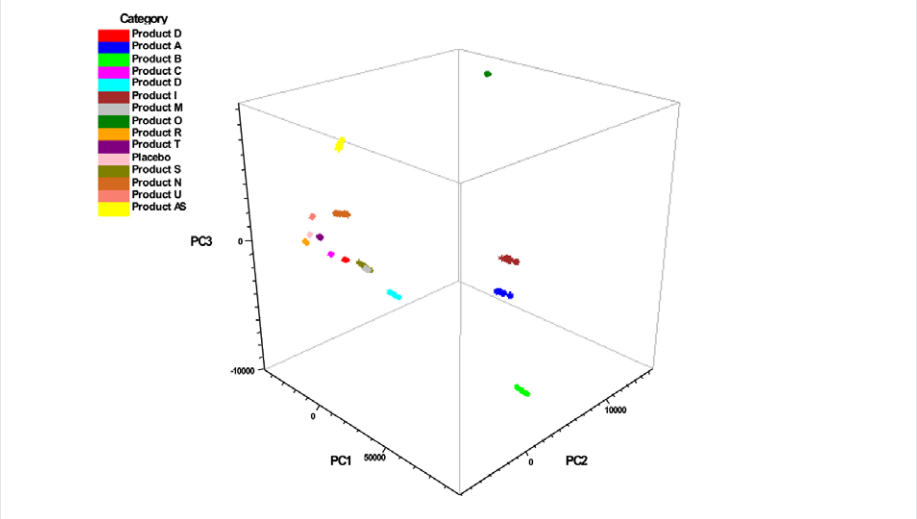

Figure 5. Analysis of preservative A and preservative B.

Samples of varying concentrations as per table 1 were acquired using the same parameters as of spectra acquired for identity test through 3 mL vial. Figure 6 is showing the spectra of the drug product with the two preservatives.

Four standards with the reference values were supplied in 3 mL and 10 mL vials and a validation sample to test the model for 3 mL and 10 mL vials.

Four spectra per standard were acquired and used to build the chemometric method. The final drug product samples were scanned with a DXR3 SmartRaman Spectrometer to acquire spectra in the range of 3500 to 50 cm-1 and captured with a single exposure of the CCD, avoiding stitching artifacts. The sample time took approximately 1 minute. Three spectra were collected per sample. The sample spectra were loaded into TQ Analyst Software for chemometric analysis using a partial least squares (PLS) method.

	Preservative A (mg/mL)	Preservative B (mg/mL)
Standard 1 3 mL and 10 mL	0.85	0.42
Standard 2 3 mL and 10 mL	1.27	1.12
Standard 3 3 mL and 10 mL	1.57	1.75
Standard 4 3 mL and 10 mL	3.07	2.57
Validation – 3 mL	1.57	1.75

Table 2. Calibration and validation sample.

	PLS results for 3 mL Cartridge	
	Preservative A (mg/mL)	Preservative B (mg/mL)
Validation sample: 3 mL	1.58 actual 1.57	1.71 actual 1.75
Real Sample in solution: 3 mL	1.56 actual 1.55	1.69 actual 1.77
Real sample in suspension: 3 mL	0.72 actual 0.69	1.23 actual 1.58

Table 3. Validation result for 3 mL sample.

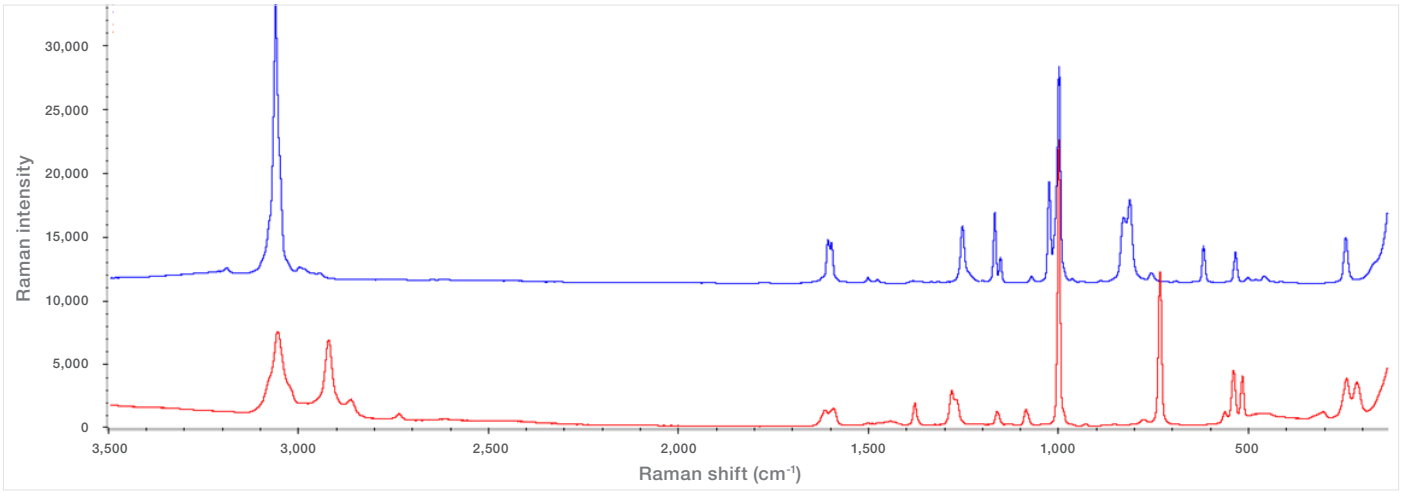

Figure 6. Spectrum in blue is from pure preservative A and spectrum in red is from pure preservative B.

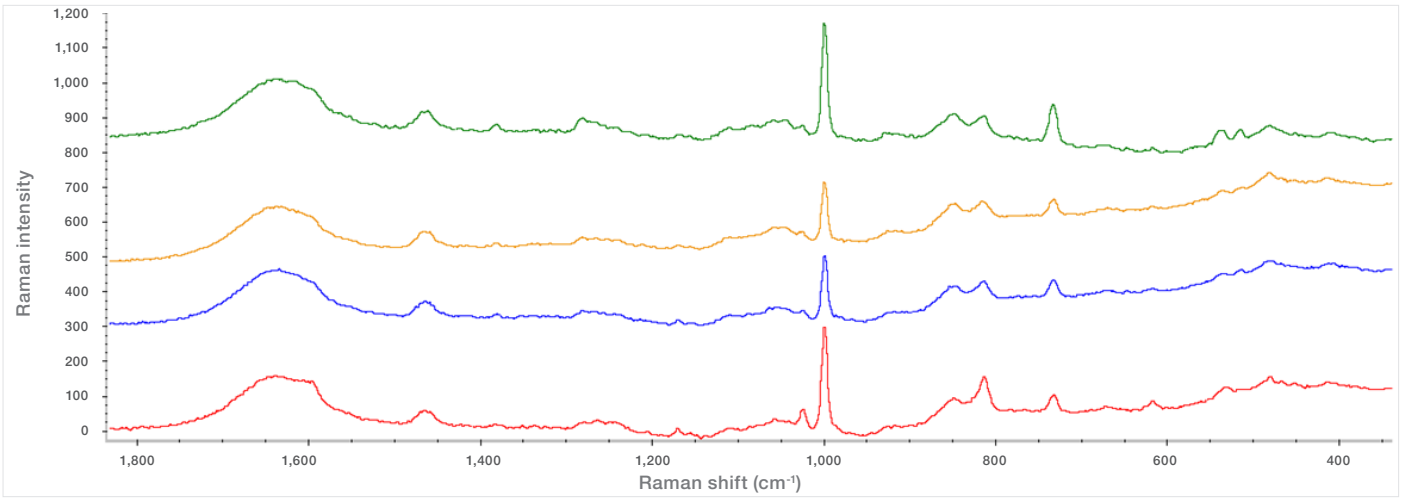

Figure 7. Spectra showing varying concentration of preservatives in final drug product.

Results

PLS analysis of the final drug product samples revealed excellent predictive capabilities within the range of materials tested. The spectra used to develop the PLS method for 3 mL cartridge are shown on calibration plots (Figure 8 and Figure 9) that compare the calculated preservative concentrations versus the actual concentrations. The calibration plot can be used to determine how well the method predicts the actual preservative concentrations in the samples. The plot developed by the chemometric method resulted in a correlation coefficient of 0.998 for preservative A. Root mean square error of calibration (RMSEC) was 0.0425 mg/mL, and the Root mean square error of prediction (RMSEP) calculated was 0.0372 for preservative A. The additional method for preservative B resulted in in a correlation coefficient of 0.999. The RMSEC was 0.0316 mg/mL, and the calculated RMSEP was 0.0496. The method was able to accurately predict the 3 mL validation sample and a real sample in solution (Table 3). The prediction can be improved when suspensions are allowed to settle and liquid phase is analyzed.

When 10 mL vial calibration samples were added to the above PLS method, method performance remained the same and was able to accurately predict the validation samples (Table 4).

Conclusions

A multi-attribute test to establish Final product identification and predicting concentrations of preservatives was done with the DXR3 SmartRaman Spectrometer by developing a discriminant analysis method and partial least square method. The final drug product identification test is part of release testing and current methods used are time-consuming and laborious. This Raman technique successfully demonstrates the ability to measure and monitor preservative concentrations either in the lab environment or at the line. The method developed shows excellent correlation with actual preservative concentrations with errors comparable to the reference analysis method. This application demonstrates the continued capability of the DXR3 Raman Spectrometer to be successfully used in bioprocess environments for implementing multi-attribute final product testing of biologics. Apart from the examples shown here, DXR3 SmartRaman Spectrometer can be used to implement at-line control strategies to monitor protein concentration, excipients concentration, and critical quality attributes like osmolality and pH. Many such examples are cited in the literature for Raman applications in biopharma manufacturing.

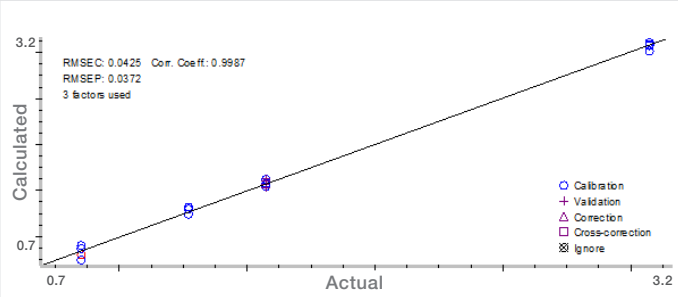

Figure 8. PLS model for preservative A —3 mL cartridge.

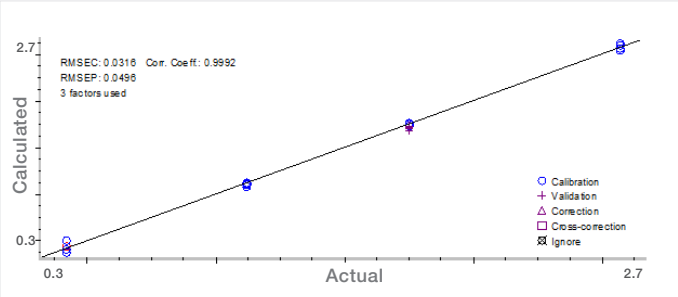

Figure 9. PLS model for preservative B —3 mL cartridge.

	PLS 3 mL cart and 10 mL vials	
	Preservative A (mg/mL)	Preservative B (mg/mL)
Validation sample: 3 mL	1.58 actual 1,57	1.71 actual 1,75
Real sample in solution: 3 mL	1.56 actual 1.55	1.65 actual 1.77
Real sample in suspension: 3 mL	0.80 actual 0.69	1.21 actual 1.58
Real sample in suspension: 10 mL	0.73 actual 0.68	1.32 actual 1.57

Table 4. Validation results for 3 mL 10 mL vials.

References:

1. European Medicines Agency. Guideline on Real Time Release Testing. https://www.ema.europa.eu/en/documents/scientific-guideline/guideline-real-time-release-testing-formerly-guideline-parametric-release-revision-1_en.pdf (accessed June 15, 2021).
2. Buckley K, Ryder AG. (2017). Applications of Raman spectroscopy in biopharmaceutical manufacturing: a short review. *Applied Spectroscopy*, 71(6): 1085-1116. https://aran.library.nuigalway.ie/handle/10379/7177 (accessed June 15, 2021).

Notes

Learn more at **thermofisher.com**

thermo scientific